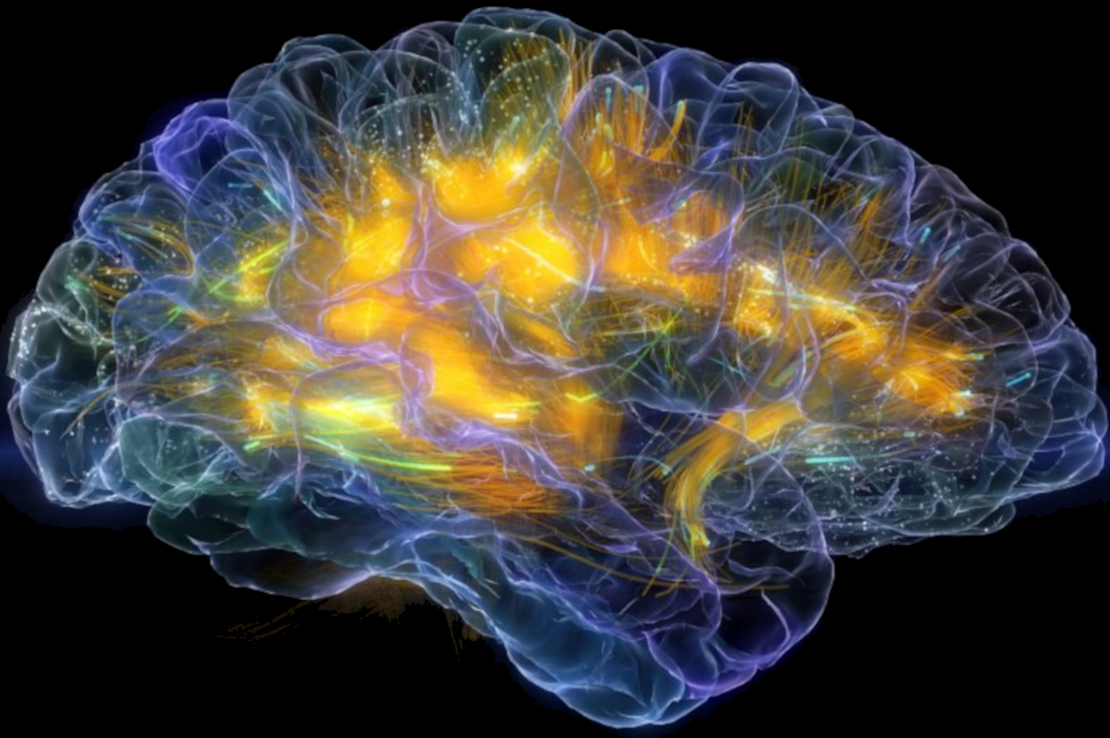


# VoNA: The Visualisation of Neuronal Activation

To observe and shape electrode-generated outputs  
for electrical stimulation in the brain using a Finite  
Element Model

Niels van Lith

Delft University of Technology



# VoNA: The Visualisation of Neuronal Activation

To observe and shape electrode-generated outputs  
for electrical stimulation in the brain using a Finite  
Element Model

by

Niels van Lith

to obtain the degree of Master of Science at the Delft University of Technology,  
to be defended publicly on 30 January 2024 at 13:00.

Student number:	4305051	
Project Duration:	January, 2022 - January, 2024	
Thesis committee:	dr. T.M.L. Costa,	TU Delft, supervisor
	MSc. F. Varkevisser	TU Delft, daily supervisor
	dr.ir. R.F. Remis	TU Delft

An electronic version of this thesis is available at <http://repository.tudelft.nl/>

Cover: Glass brain image. Made by Neuroscape, UCSF. (Modified)

# Acknowledgements

It would not be an understatement to call my journey at the TU Delft an academic endeavour that would not have been possible without the guidance and support of many people. I could not have finished this project alone, and I am very thankful to all who helped me, whether in good or sometimes less accommodating times. To everyone in the Bioelectronics group: Thank you! You ensured everyone was welcome, and your activities, coffee breaks and meetings have shown me that so much excellent work is being done on the 16th floor. I am glad that I could be a part of that. A special thanks to Tiago and Cesc for their supervision during my project as well as for their faith in what I was doing, especially as I could be stubborn at times..

To my friends and family, thank you for your unwavering support and encouragement throughout this academic journey. This would have been much less fun without you, and I am pretty sure I would not have made it this far.

*Let this project prove that even those with a fear of failure can move mountains as long as they keep trying.  
You can always do more than you initially expect*

*Niels van Lith  
Delft, January 2024*

# Summary

The development of neural prostheses, especially those directly targetting the brain, requires extensive research and modelling before clinical trials can be performed. Currently, the resolution of artificial vision is not sufficient for everyday tasks. By studying the expected spatial extent of stimulation, we hope to provide insights to researchers that can be used to improve the resolution of artificial vision. The goal of this MSc thesis was to visualise the shape and intensity of electric fields in the cortex as a response to intracortical microelectrode stimulation to observe the expected regions of neuronal activation considering electrode design parameters. To do this, parameters that can influence the generated electric field and the regions of activated tissue have been defined. Implementing these parameters in a Finite Element Model (FEM) allows the computation of the generated electric field in 3D of a stimulating electrode to observe the spatial extent of activated tissue. The spatial extent of activated tissue can be estimated using simplified methods such as the activating function (AF) or the strength-distance relation. The result is a parameterised framework that creates a Visualisation of Neuronal Activation (VoNA) that can be used to assess activated tissue regions for varying scenarios by defining material properties and dimensions of the model, and allows for the adjustment of the stimulation configuration, electrode contact spacing, customisation of electrode size and modulation of stimulation current. It enables the user to tune the model settings towards their specific needs and explore the possibilities by visualising the results from different angles by defining subsets of the entire solution.

In line with expectations, the presented models show that the model parameters can influence factors such as the generated electric field, the current density and electric potential, which are indicators of neuronal activation. The findings support the hypothesis that these parameters should be considered during electrode design to achieve accurate stimulation.



# Contents

<b>Preface</b>	<b>i</b>
<b>Summary</b>	<b>ii</b>
<b>1 Introduction</b>	<b>1</b>
1.1 Background . . . . .	1
1.1.1 Visual processing . . . . .	1
1.1.2 Neuromodulation . . . . .	3
1.1.3 Restoring vision . . . . .	6
1.2 Problem statement . . . . .	7
1.3 Report outline . . . . .	8
<b>2 Literature Review</b>	<b>9</b>
2.1 Modelling neuronal excitation . . . . .	9
2.2 Estimating the spatial extent of neuronal activation . . . . .	10
2.2.1 The strength-distance equation . . . . .	10
2.2.2 Activating Function . . . . .	11
2.3 The current state of the intracortical visual prosthesis . . . . .	12
2.4 The challenges and considerations of intracortical prostheses . . . . .	13
2.4.1 Resolution of artificial vision . . . . .	13
2.4.2 Image processing . . . . .	13
2.4.3 Wireless power and data transmission . . . . .	14
2.4.4 Long-term stability and biocompatibility . . . . .	14
2.4.5 Electrode Tissue Interface . . . . .	15
2.5 Electrode design models and considerations . . . . .	15
2.5.1 Considerations in electrode design . . . . .	16
2.5.2 Existing computational models for electrical stimulation . . . . .	16
2.6 Thesis objective . . . . .	17
<b>3 Method</b>	<b>18</b>
3.1 Model description . . . . .	18
3.2 Model output . . . . .	19
3.3 Evaluation of the spatial extent of stimulation . . . . .	20
<b>4 Results</b>	<b>22</b>
4.1 VoNA: the Visualisation of Neuronal Activation . . . . .	22
4.2 Observing the generated electric potential . . . . .	26
4.3 Influence of the electrode contact pitch . . . . .	28
4.4 Electric fields and their gradients . . . . .	28
4.5 Estimating neuronal activation using surface current density . . . . .	31
4.6 Neuronal activation using the activating function . . . . .	32
<b>5 Discussion &amp; Conclusion</b>	<b>36</b>
5.1 Observations on the Influence of Model Parameters . . . . .	36
5.1.1 The Influence on the Electric Potential, Field and Current Density . . . . .	36
5.1.2 The influence on the current-distance relation and the activating function . . . . .	37
5.2 Model setup and limitations . . . . .	37
5.3 Conclusion . . . . .	37
5.4 Recommendations for future work . . . . .	38
5.4.1 The implementation of the electrode tissue interface . . . . .	38
5.4.2 Adding glial scar encapsulation . . . . .	38
5.4.3 Validation against other approaches . . . . .	38

---

5.4.4	The addition of a time-dependent simulation . . . . .	38
5.4.5	Improving the application of the activating function . . . . .	38
5.4.6	Simulation of multiple electrode shanks . . . . .	38
5.4.7	Adding more electrode contact parameters . . . . .	38
<b>References</b>		<b>39</b>

# Introduction

Our senses play a crucial role in how we experience the world – from hearing and smelling to tasting, feeling, and seeing. Unfortunately, all over the world, people face disorders that affect their senses, like hearing loss or visual impairments. All information obtained by the senses is processed in the brain. Currently, research is done on developing neural prostheses - devices that can aid or replace damaged neuronal functions due to accidents or diseases using neuromodulation [1]. The devices interact with nerves in the body by delivering a form of stimulation directly to a target area. Various forms of stimulation can be applied to interact with nerves. These methods vary from chemical applications, leveraging properties associated with the thermal domain, optical interventions, and mechanical approaches. Research is being done on applying these domains, where the most conventional application of treating diseases uses drugs. But, when drugs are ineffective, a common alternative is to apply stimulation through the application of electrical pulses [2].

Neural prostheses have shown promise in treating various neurological conditions. For instance, cardiac pacemakers help with heart arrhythmia [3], cochlear implants aid those with hearing disabilities [4], and deep brain stimulators alleviate tremors in diseases like Parkinson's disease [5]. The obtained knowledge is being used to treat patients with visual impairment by developing a visual prosthesis that could be used to restore some form of vision [6]. However, more research is needed before visual prostheses are ready for practical use. The devices must be able to produce an artificial vision that has high spatial resolution. Currently, the resolution is low, reducing its usefulness for everyday tasks [7]. The achieved resolution depends on several factors. Take, for example, the intensity or duration of stimulation, the placement of the electrode, as well as the electrode properties [8]. Researchers are developing prostheses that directly stimulate the brain through microelectrodes to improve spatial resolution by increasing the density of stimulation electrodes and their ability to achieve sufficient spatial resolution [9]. To advance ongoing research, it is essential to simulate and visualise how design variables such as electrode properties affect the electric field's spread within the brain. To the author's knowledge, a tool that offers flexibility for visualising the effect of electrode properties is still unavailable.

This MSc thesis presents a visualisation framework that can be used to study the expected activated regions of neurons using a Finite Element Model (FEM) for intracortical stimulation. The result is a tool that allows researchers to examine the effects of changes in their electrode designs to improve the spatial resolution of artificial vision. The framework is designed in the context of visual prostheses, but it can be used as a general framework for neurostimulation regardless of the application or stimulation location.

## 1.1. Background

To understand how visual prostheses provide a solution for those with a visual impairment, one should form a basis on the human processing of visual information and neuromodulation.

### 1.1.1. Visual processing

Perceiving our surroundings starts with the arrival of light into the eyes. The retina, located at the back of the eye, contains photoreceptor cells - rods and cones - which respond to light stimuli and transmit signals through the bipolar cells to the ganglion cells. The ganglion cells then converge to form the optic nerve [10]. The optic nerve acts as a conduit, transmitting vast amounts of visual information to the brain. Before the information

reaches the primary visual cortex, it passes through the thalamus's lateral geniculate nucleus (LGN) [11]. The relay of visual communication, described as the visual pathway, is illustrated in Figure 1.1.

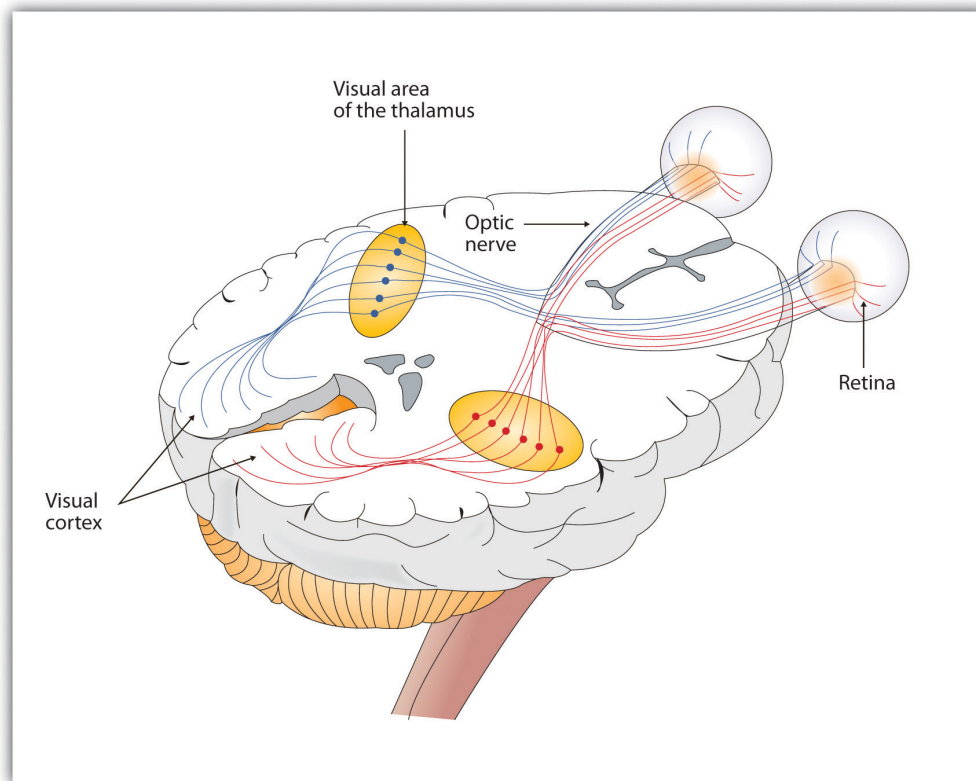


**Figure 1.1:** Illustration of the human visual pathway from retina to the visual cortex. Figure obtained from [12]

The visual cortex is the cerebral cortex region in the occipital lobe at the posterior side of the brain. It plays a role in perceiving and interpreting visual stimuli, encompassing colour, shape, motion, and depth. The visual cortex is subdivided into five distinct regions (V1–V5), and the first three regions are shown in Figure 1.2a.

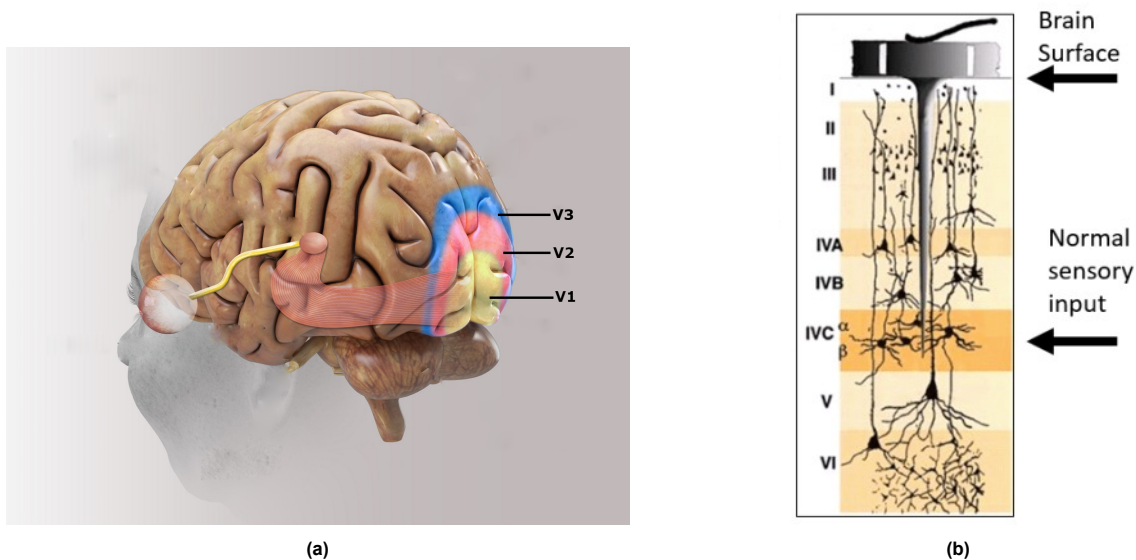


**Figure 1.2:** (a) An illustration of the first three regions of the visual cortex. V1, V2, and V3 are indicated in yellow, red, and blue, respectively. (b) Distinct layers of the neocortex. Visual sensory input enters V1 at layer IVc. Figures adapted from [13] and [14]

Each region specialises in distinct visual functions. For instance, V1 is primarily involved in basic visual processing. The brain systematically organises visual information using retinotopic mapping [15]. This principle ensures that the brain retains spatial relationships of visual information received from the retina [16]. As information progresses from V1 to V5, it becomes increasingly abstract [14]. The information is not processed only on the surface of each region. The cerebral cortex consists of two layers. The brain's outermost layer is the neocortex, which is responsible for performing cognitive functions [10]. The neocortex consists of cortical columns, each organised into six distinct layers with neuronal cell types, functions, and connectivity patterns [17–19]. Each column performs its function, explaining how the regions V1 - V5 can perform differently. The division of the neocortex in layers, from surface layer I to deepest layer VI, is shown in Figure 1.2b. Visual information from the LGN arrives at the visual cortex at layer IVC [20].

For the brain to perform complex tasks, it enables different cortical columns to communicate and share information through Canonical Cortical Circuits (CCC). These CCCs consist of horizontal neuronal circuits running parallel to the neocortex's surface, creating the ability to integrate data from different sources to execute complex cognitive functions [17].

### 1.1.2. Neuromodulation

With the basics of visual processing in humans explained, the next step is understanding the concept behind neuromodulation: neuronal excitation.

#### Neuronal excitation

Neural prostheses apply electrical stimulation to interact with the nervous system. Specifically, they stimulate nerve cells [19]. Nerve cells, also called neurons, can be electrically and chemically stimulated and are responsible for transmitting electrical signals throughout the body. A typical neuron is shown in Figure 1.3.

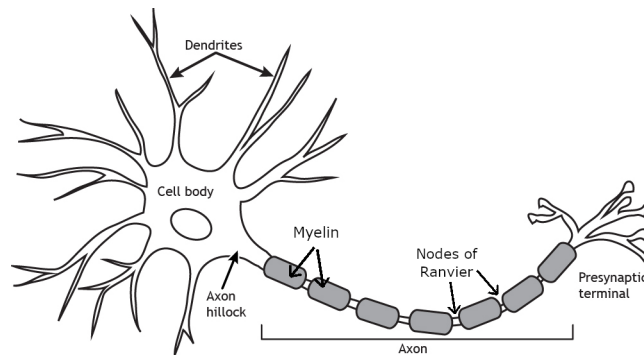


**Figure 1.3:** The structure of a typical neuron. Image is an adaptation of [21]

The neuron cell body, called the soma, has two types of extensions. The first are the dendrites, which receive signals from other neurons. The other extension is the axon, which conducts an electrical signal, called an action potential, towards the presynaptic terminal. The axon can be covered by an insulation layer called myelin to increase the action potential's propagation speed [22]. Along the length of the axon intersections will be created, so-called nodes of Ranvier [23]. When an action potential reaches the terminal, neurotransmitters are released. Neurotransmitters are chemicals used to activate or inhibit the receiving nerve cell, setting up communication with surrounding cells.

Communication between neurons is dependent on the presence of action potentials. The action potential is an all-or-nothing reaction due to a cell's membrane electric potential shift. A lipid bilayer membrane forms the walls of a nerve cell [23]. This membrane contains proteins that form channels to connect the inside and outside of the cell. An example of ions that can pass through the membrane are potassium ( $K^+$ ) and sodium ions ( $Na^+$ ). Due to a difference in ion concentrations between the interior and exterior of the cell, an electric potential difference is created called the membrane potential  $V_m$ . The protein channels regulate the concentrations of ions in the cell. At rest, the membrane potential is kept around -70 mV to -80 mV [24].

When neurotransmitters reach the dendrites or soma of a nerve cell, they encourage some of the protein channels to react. The protein channel reaction depends on the electrical potential difference across the cell membrane, opening up or closing briefly. The reaction creates a diffusion of particles, changing the ion concentrations in and outside the cell, affecting the membrane potential. When the membrane potential

depolarises, the electrical potential difference becomes smaller, and the opposite of depolarisation is called hyperpolarisation, where the potential difference increases to a more negative value. This behaviour and the all-or-nothing reaction of the action potential are shown in Figure 1.4.

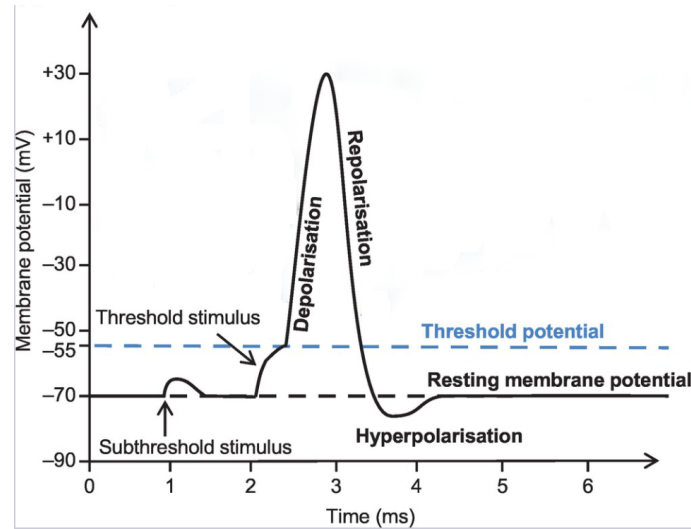


**Figure 1.4:** An example of an action potential. It shows a membrane at rest, which then receives a stimulus that initiates a depolarisation of the membrane potential. The all-or-nothing reaction will start when the depolarisation crosses the threshold. While the cell repolarises, it can not react to any stimulus until it returns to the resting potential. Image is an adaptation of [25]

When the depolarization exceeds a certain threshold, it will prevent the cell from returning to a steady state for a moment. It creates a chain reaction which travels along the entire neuron. An action potential has been generated. While this chain reaction occurs, the neuron cannot respond to any change until the event has finished. After the action potential, the neuron enters a repolarisation process to return to its steady-state solution.

### Electrical stimulation

Neural prostheses apply electrical stimulation to interact with the nervous system. This interaction generates an electrical field after applying a potential or current pulse at an electrode near the cell. The resulting electric field exerts a force on charged particles, which triggers a reaction from the potential-gated channel proteins. Under normal circumstances, the membrane prevents depolarization using the regulation of ions. However, when the applied electric field is strong enough, the membrane can not keep up with the change in the membrane potential; an action potential is triggered. Research shows that direct neuron activation sites are most often found at the nodes of Ranvier. The nodes contain high concentrations of sodium channels, making them the most excitable neuron segments [26].

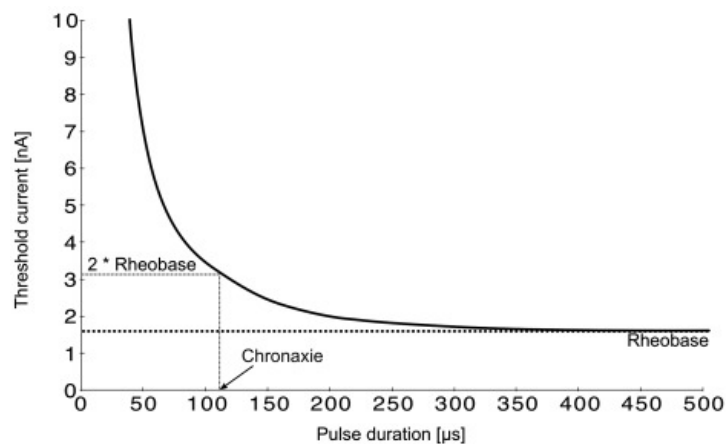


**Figure 1.5:** A strength-duration curve for nerve stimulation. The curve shows a chronaxie of  $\sim 120 \mu\text{s}$ . Image obtained from [23]

The relation between current amplitude and time to achieve activation, known as the strength-duration curve [27], is shown in Figure 1.5. The minimal amount of current needed for initiating an action potential, assuming that it is applied for an infinite duration of time, is represented by the rheobase current [23]. The chronaxie expresses relative excitability. It represents the time needed to reach activation when applying a current amplitude twice the rheobase current and is a measure of sensitivity. Shorter chronaxies equal easier excitable neurons. The rheobase current and chronaxie values depend on tissue properties such as cell membrane thickness [27].

Effective stimulation can be achieved by defining parameters such as the applied waveform, the stimulation method, the electrode placement, the electrode contact size and the used materials. The applied pulse can be varied using different polarities, stimulation duration, frequencies and amplitude. The effect of the waveform parameters and stimulation method have been researched extensively [28]. The waveform parameters and stimulation method are related to the safety and power efficiency of stimulation of the visual prostheses [29]. These considerations are relevant during prostheses design but do not fall within this project's scope. This thesis focuses on the influence of the properties related to the design of electrodes, e.g. the configuration, placement and electrode materials on the volume of stimulated tissue, as these properties are still being studied [8].

### Electrode configuration

Stimulation by electrodes can be done by connecting a current source to two electrodes placed in tissue to apply a current pulse. During the pulse, current enters the tissue through one electrode, the stimulation electrode, and returns through the return electrode. The positive electrode, the anode, attracts negative charges, while the negative electrode, the cathode, attracts positive charges. The distance between the electrodes and the number of used contacts influences the resulting electrical field. For example, placing the stimulating electrode close to the cell that is to be activated and placing the return electrode at a considerable distance away will result in a broad electrical field. The stimulation may target neighbouring neurons, resulting in a low spatial resolution. This configuration of placing the electrodes is known as a monopolar electrode configuration. The resulting electric field will be spherical if this configuration is placed in an electrically homogeneous solution. The resulting potential and current are shown in the left panels of Figure 1.6. The panels show the regions that have the potential as isopotential circles. Black arrows indicate the direction of the current flow.

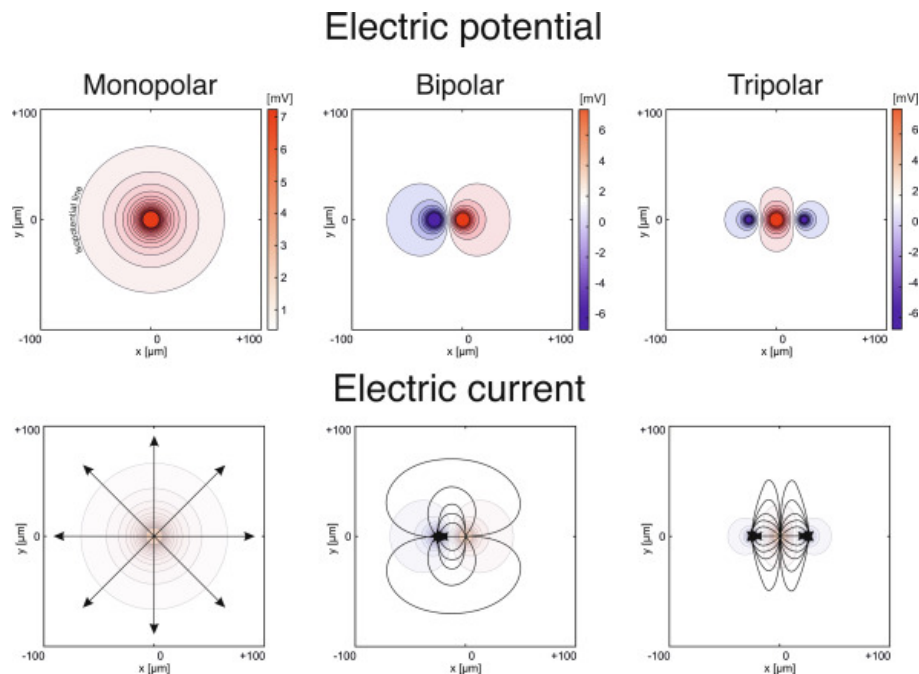


**Figure 1.6:** Potential distribution for electrodes placed in a plane of infinite homogeneous brain tissue. The circles show regions of the same potential, and the arrows show examples of the current flow. The results are shown for a monopolar, bipolar, and tripolar configuration. The Monopolar configuration shows a symmetric electric field that spreads out circularly. The bipolar configuration shows a more confined electric field. The currents are focused between the working and return electrodes, creating an asymmetric electric field. The tripolar configuration is even more focused, increasing the asymmetry of the field while reducing the covered area. Image obtained from [30]

The electrodes can be placed close to each other to generate a more focused stimulation. The influence of stimulation will be focused in the region between the electrodes, reducing the spread and increasing the spatial resolution. This configuration is called a bipolar electrode configuration, as both electrodes affect the tissue. The resulting potential and current are shown in the centre panels of Figure 1.6. There are more possibilities aside from these two configurations. The applied electric field can be influenced by increasing the number of electrodes, creating a multipolar electrode configuration. This effect is shown in the right panels of Figure 1.6 using a tripolar (three electrodes) configuration. Dividing the electrical field using two return electrodes confines the affected region even more. If electrodes have identical applied stimulation amplitudes (current or electric potential), the electric field's peak is found between the two electrodes. This peak shifts when one electrode has a different amplitude, moving towards the electrode with a higher amplitude. The contributions of each electrode overlap, "steering" it to create a virtual electrode, allowing the creation of more favourable stimulation patterns. This concept is known as current steering [31, 32].

### 1.1.3. Restoring vision

Loss of vision results from damage, be it due to a disease or accident, to any part of the visual pathway (as described in subsection 1.1.1). To aid patients, prostheses are being developed to restore vision [33, 34]. With the basics of visual processing and the concept behind neuromodulation explained, the final step is to explain how visual prostheses are used to restore vision.

A visual prosthesis operates on the idea of bypassing the damaged portion of the visual pathway by directly stimulating intact neurons [34, 35]. An external wearable device registers visual input, often a camera mounted on glasses. The information is processed using software to be transmitted to an electrode array to stimulate a part of the visual pathway to create spots of light known as phosphenes [36]. Phosphenes are a perception of a ring, or area, of light that can be mapped to form a visual map [37]. The electrical stimulation can happen at various locations along the visual pathway. For example, the retina, the optic nerve, the lateral geniculate nucleus (LGN) or the primary layers of the visual cortex [37]. This is shown in Figure 1.7.

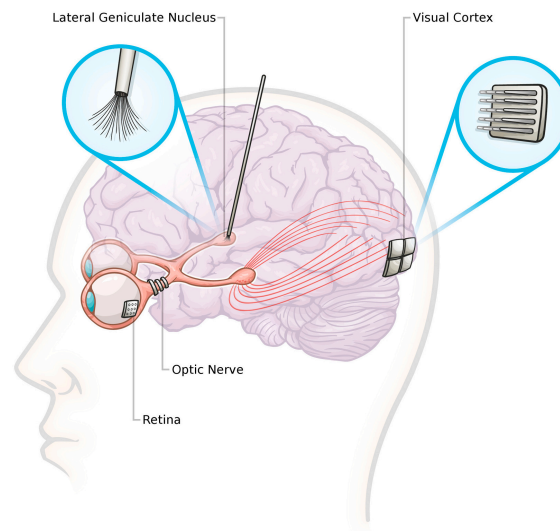


**Figure 1.7:** Possible targets for stimulation of a visual prosthesis. Image obtained from [37]

The prostheses highlighted in this thesis stimulate the visual cortex instead of the other locations. The primary target for implantation of electrode arrays is the region V1 of the visual cortex [26]. Stimulating the visual cortex is beneficial. Targeting the visual cortex makes it possible to treat blindness caused anywhere along the visual pathway since the last stage of the path is being stimulated [38]. In contrast, other approaches, like retinal implants, are limited in treating causes of blindness beyond the retina [39]. Another benefit is that region V1 has uniform thickness and cell density for central and peripheral vision. It has a well-organized visuotopic map [39], and the visual cortex offers a larger space for implanting electrodes compared to other locations, such as the retina or LGN [37]. This allows more electrodes to be implanted, creating more phosphenes enabling higher resolution images [14].

For cortical visual prostheses, layer 4c is targeted due to its relatively low signal abstraction [14]. Two main approaches for electrically stimulating neurons are considered: cortical surface stimulation using planar elec-



trodes and intracortical stimulation with penetrating electrodes. While surface electrodes cause less damage to brain tissue, they require stimulation current amplitudes that are several orders of magnitude higher, which can lead to undesirable effects such as generating multiple phosphenes, cross-talk, or epileptic seizures [38]. Therefore, intracortical electrodes, despite being more invasive, are preferred due to their ability to achieve stimulation with lower amplitudes.

By generating multiple phosphenes at locations determined by the brain's visual map, an artificial grid-like vision can be created [34, 40]. Higher quality images can be achieved by creating more phosphenes. An example is shown in Figure 1.8. Increasing the number of available electrodes allows for the creation of high-quality images. However, a higher electrode density will not always achieve a better spatial resolution. Electrodes close to each other can produce identical or similar phosphenes that patients cannot meaningfully distinguish between them [9]. The requirements to evoke a phosphene depend on several factors. For example, the shape and intensity of phosphenes depend on the stimulus's amplitude and pulse width. The threshold for activation depends on the electrode impedance and placement and differs between electrodes and over time [41]. Therefore, to improve the quality of artificial images, the spatial resolution of the stimulation must be improved. Improving the resolution can be done by selectively stimulating neurons and avoiding overlap.

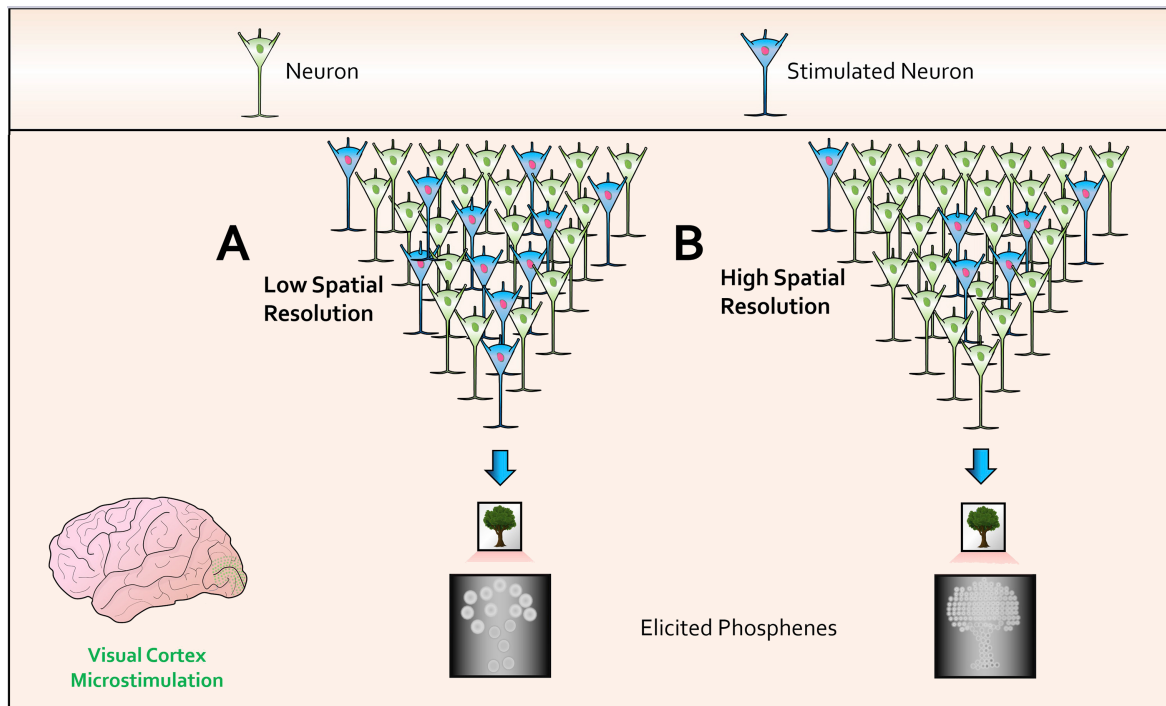


**Figure 1.8:** An example of artificially generated images of visual neuroprostheses and the effect of spatial resolution. (A) Stimulation with a low spatial resolution creates blurry images. (B) High spatial resolution allows for higher-quality images. Image is an adaptation of [42]

## 1.2. Problem statement

Intracortical prostheses are being developed to restore vision in individuals with visual impairments. These devices need to be small in size, durable over long periods of implantation life, and able to confine activation to small, local regions to achieve sufficient resolution of phosphenes. However, resolution is constrained by various limitations, which must be overcome to create devices suitable for daily use.

There is a need to adequately confine the electric field generated by electrodes to focal regions. They are affecting a broader area of neurons than necessary. As a result, the stimulation activates the targeted neurons and the interconnecting neurons that communicate with other sites. Stimulating the interconnecting neurons interferes with visual information processing. The processing does not occur in a single, precisely defined area of the brain but in various parts of the visual cortex. Thus, activating more areas than needed will diminish the ability to restore high-acuity vision. Greater control over the shape of the electric fields and their impact on stimulation spread is wanted while considering the relation with electrode design parameters. Therefore, this project aims to develop a tool to visualize the electric fields created by electrodes.

Given this problem statement, this thesis addresses the following research question:

*How to visualize the shape and intensity of electric fields in the cortex, considering electrode design parameters, to observe the expected activation region?*

### 1.3. Report outline

The organisation of this thesis is set up as follows; chapter 2 presents a literature review on intracortical visual neurostimulators, the models and estimation of neuronal excitation, the properties of electrode models and developed electrode models. After the literature review, chapter 3 discusses the approach to setting up the visualisation model, the generated model output, and the evaluation of spatial stimulation. A showcase of the designed tool and output results are then discussed in chapter 4. The discussion of this framework and results will be presented in chapter 5. At the end of that chapter section 5.3 shall present a conclusion and recommendations for future work.

# 2

## Literature Review

The background information of chapter 1 provides context on using visual prostheses. The next step is to create an overview of the current state of intracortical prostheses and the related theories to address the problem statement. This chapter provides a literature review split into five parts to cover the insights related to the current state of the art. The first part discusses modelling neuronal activation, whereas the second part explains techniques that can be used to estimate neuronal activation. Following this discussion are examples of in-development visual prostheses and the related challenges and (safety) considerations. The final section describes what electrode properties can influence stimulation and describes models that have already been developed to explain the need to design the proposed framework.

### 2.1. Modelling neuronal excitation

The most common approach to simulating the neural response to electrical stimulation is a hybrid approach, which uses a multi-compartment model in combination with an approximation of the extracellular potential [43]. The multi-compartment models are cell membrane models, primarily based on cable theory [44], that describe the change in the voltage across the cell membrane as a function of time. This description is implemented via differential equations that describe the ionic currents flowing through the cell membrane. To do this, a

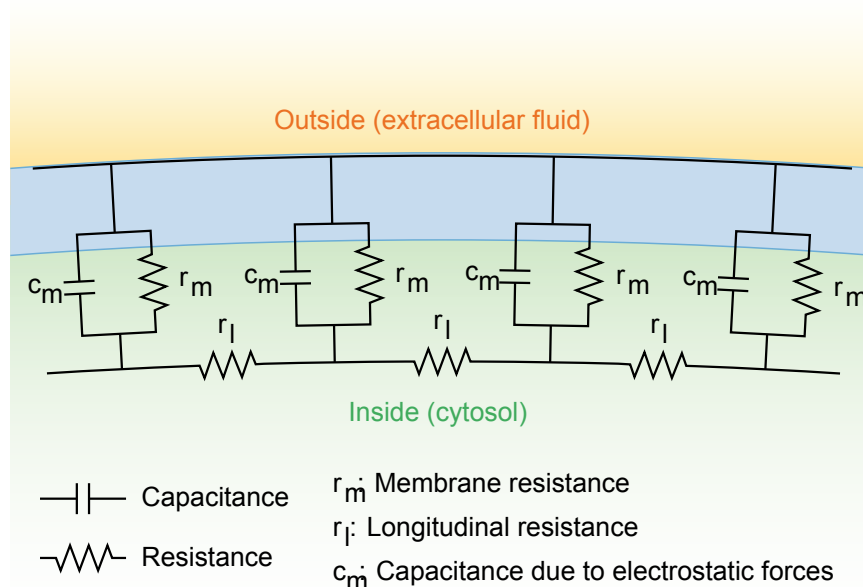


**Figure 2.1:** A simplified schematic representation of a neuron according to cable theory. Figure obtained from [45]

neuron is divided into distinct compartments containing electrical elements, representing small segments or

sections of the neuron, as shown in Figure 2.1. In this way, a model of the neuron is formed that acts as a closed electrical circuit, which can be evaluated considering Kirchhoff's laws [46]. The extracellular potential  $V_e$  is required to solve a multi-compartment model. The potential is determined by calculating the electric field generated by a stimulating electrode using an analytical approximation or numerical approach using a finite element model (FEM) [47]. Free software solutions like NEURON are widely used to solve multi-compartment models.

An alternative strategy to model the neural response is the use of a 'whole FEM approach' where the calculation of the extracellular and intracellular potentials happen simultaneously via FEM software [48]. The 'whole FEM approach' allows physical interactions between the neuron and its environment to be modelled for every point in space and time. An example of this setup is shown in Figure 2.2 Depending on the FEM software, the simulation might consider additional physics, like electrode impedances or tissue permittivity. In the 'whole FEM approach', the cell geometry is fully realized in 3D and does not have the geometric limitations of a multi-compartment model. However, while this approach eliminates geometric limitations, it comes with downsides such as high computational costs, increased model complexity /development and the expense of professional FEM software solutions. This method is currently too computationally intensive to be practical for most clinical applications. Therefore, simplified methods for calculating the spatial extent of axonal activation have been developed and will be discussed in section 2.2.

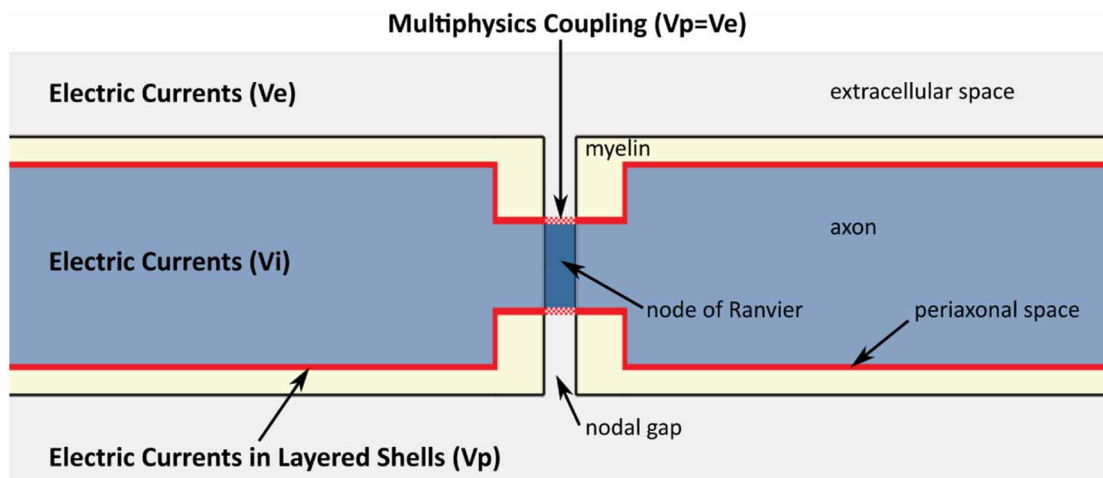


**Figure 2.2:** An illustration of the implementation of a neuron in a whole FEM model by defining both the intra- and extracellular properties. The properties that are used in the multi-compartment model are still there but are now linked to the physics of the FEM. Image obtained from [49].

## 2.2. Estimating the spatial extent of neuronal activation

As mentioned in section 2.1, methods have been developed to calculate the spatial extent of neuronal activation using certain simplifications that researchers can use to gain insight. This section discusses two of the most commonly used methods: the strength-distance equation and the Activating Function (AF).

### 2.2.1. The strength-distance equation

The first method to determine the spatial extent of neuronal activation is based on visualising the generated current density in space since it indicates effective current spread in the medium. By visualising this current spread, information can be obtained about the volume where neuronal activation is possible, which is useful when information is lacking concerning geometry or properties of the involved neural structures [43]. The effective spread is determined by observing whether the measured current density in a specific volume reaches or exceeds a set current density threshold. This current density threshold, introduced as the excitability constant  $K$ , differs for the used medium and is derived from experimental data. Applying a current equal to the excitability constant indicates that a neuronal element located 1 mm from the electrode contact has a probability of 50% to trigger an action potential [26]. Tissue associated with an average constant of  $K = 1292 \text{ } [\mu\text{A}/\text{mm}^2]$  would require  $1292 \text{ } \mu\text{A}$  of current for activation when positioned 1 mm away.

$$I = Kr^2 \text{ } [\mu\text{A}] \quad (2.1)$$

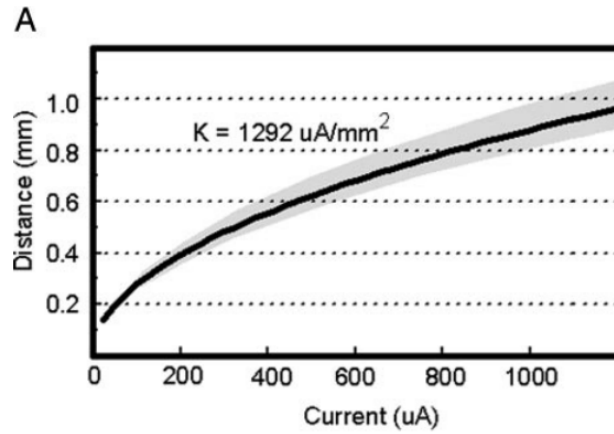


**Figure 2.3:** direct activation of neurons using the effective current spread equation. The curve represents the amount of current required for an action potential. In this example, the average value for  $K$  was  $1,292 \mu A/mm^2$ . Figure is an adaptation from [26]

The strength-distance relationship is described by Equation 2.1 and illustrated in Figure 2.3. The relation shows that the effective spread mainly depends on the magnitude of the applied current since the average excitability constant depends on the tissue that is being stimulated. For instance, the average excitability constant of tissue in the visual region V1 has a value of  $K = 675 \mu A/mm^2$  [17], while the average of tissue in the cerebral cortex is  $K = 1292 \mu A/mm^2$  [26]. Studies have revealed an inverse correlation between the excitability constant, the size of a neuron's axon, and whether it is myelinated [28]. Higher conduction velocities lead to lower threshold values [17]. Smaller regions of expected stimulation shall be observed when stimulating non-myelinated tissue.

### 2.2.2. Activating Function

The AF is the second method to assess the spatial extent of neuronal activation. It is a function that describes the non-linear relationship between a neuron's input current and output voltage by observing the spatial derivative of the electric potential along a nerve [50] and is a fairly accurate predictor for stimulation [51]. The spatial derivative can be used to determine whether depolarization that surpasses the required threshold to trigger an action potential is present, as the most significant excitation occurs where the largest gradient (change) along the neuronal structures is found. The AF is expressed as Equation 2.2 and is based on the cable theory model of a neuron.

$$f_n = \frac{d}{4c_m \cdot \rho_i} \cdot \frac{V_{e,n-1} - 2V_{e,n} + V_{e,n+1}}{\Delta x^2} \quad [\mu A/mm^2] \quad (2.2)$$

In the equation,  $d$  represents the diameter of the axon (typically between  $10 \mu m$  and  $1 \mu m$ ),  $c_m$  is the membrane capacitance per square unit area ( $1 \mu F/cm^2$ ),  $\rho_i$  is the resistivity of axoplasm ( $300 \Omega \cdot cm$ ),  $\Delta x$  is the distance between the measurement locations, and  $V_{e,n}$  represents the external potential at the location [52]. The AF can be interpreted as a virtual current injected near the axon or node of Ranvier. A positive current tends to depolarise the axon, whereas a negative current tends to hyperpolarise. When the virtual current exceeds the threshold, nerves will be activated due to depolarisation [43]. This equation can be simplified to form the equation shown in Equation 2.3.

$$f_n = \frac{d}{4c_m \cdot \rho_i} \cdot \frac{V_e^2}{dx^2} \quad [\mu A/mm^2] \quad (2.3)$$

When stimulating, a current source is connected to two electrodes placed in the tissue to apply stimulation. The current enters the tissue through the stimulation electrode and returns through the return electrode. By aligning the path of the current with the axon's propagation direction, a more favourable condition for stimulation can be created [30]. The regions of hyperpolarisation and depolarisation in the membrane are then further apart, preventing them from cancelling each other. This is illustrated in Figure 2.4.

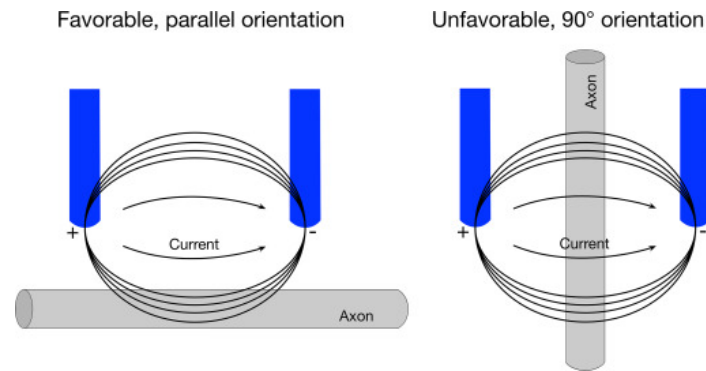


**Figure 2.4:** An example of the current path's favourable and unfavourable orientation. In the unfavourable orientation, the areas of hyperpolarisation and depolarisation in the axon are close, possibly cancelling each other's effects. Image obtained from [30]

## 2.3. The current state of the intracortical visual prosthesis

Several ongoing projects are working on applying intracortical stimulation to develop visual prostheses. Three of these projects are currently conducting clinical trials [53, 54]. One of the projects is the intracortical Visual Prosthesis Project (ICVP) at the Illinois University of Technology [55], which successfully implanted its prosthesis in its first participant in 2022. The second project is the GENNARIS bionic vision system, developed by Monash Vision Group and supported by the Australian Research Council [56]. Results of their clinical trials, published in 2020, show that long-term implantation of a visual prosthesis can be achieved without significant tissue damage [57]. The third project is the Cortical visual prosthesis for blind people named CORTIVIS, which the European Commission supports [58] and uses the Utah Electrode Array (UEA), which has been approved by the Food and Drug Administration (FDA) for long-term human studies [35].

The general design of these projects is similar; they capture visual information through a camera, which is then processed through a video processing unit to be converted to a sequence of commands that are transferred to the array(s) of implanted electrodes of the prosthesis [59]. An example of the general design of a wireless intracortical prosthesis is shown in Figure 2.5.

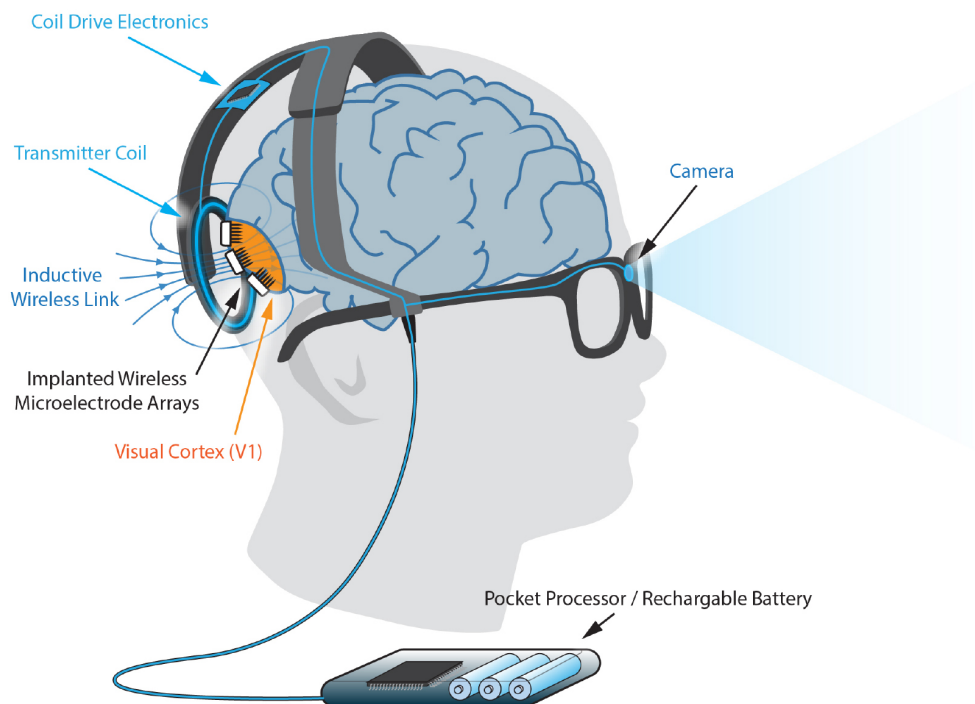


**Figure 2.5:** An example of an intracortical visual prosthesis. The prosthesis uses an embedded camera to capture images, which an external pocket processor processes to generate instructions. The instructions and power are delivered to the microelectrode arrays through a wireless inductive link. The image shows the implementation of the GENNARIS project and is obtained from [60].

The projects distinguish themselves in the implementation of their intracortical prostheses. For example, they use different quantities of electrodes per array that are used to stimulate, e.g. 100 electrodes for the CORTIVIS project, 16 for the ICVP project or 43 electrodes for the GENNARIS project [53]. They also vary in the dimensions of the designed implants, as the UTAH electrode array is a flat rectangle of 4 mm by 4 mm [58], where the electrode array of ICVP is a 2 mm by 2 mm tile [55] and the array of GENNARIS is located on a 9 mm × 9 mm tile [60]. Something noteworthy is that the developed systems of the ICVP and GENNARIS Project do not use a single array but cover the visual cortex with several tiles containing electrodes of different lengths, a receiver coil, and an application-specific integrated circuit (ASIC). Each electrode array can be controlled individually through the ASIC while powered by a single transmitter. Using these tiles, the ICVP anticipates that if the clinical trials go as expected, with the available space, implantation of up to 600 electrodes is possible [55]. The GENNARIS project supports up to 473 stimulating electrodes [60]. These projects showcase different approaches to advancing artificial vision, but although progress is being made, challenges must be resolved before the prostheses can be used as practical devices.

## 2.4. The challenges and considerations of intracortical prostheses

The projects from section 2.3 show the potential of intracortical prostheses in preclinical and clinical testing. However, artificial vision does not allow the patient to regain total functional vision due to technological and biological limitations [1, 37, 38, 53]. In the review by E. Borda and D. Ghezzi [53], the limitations are expressed as influences on the visual field size, the spatial resolution and the temporal resolution of the generated images. Visual prostheses should provide higher resolution and broader angles of the visual field to help patients perform daily activities. While beyond the scope of this thesis, there are also challenges related to ethics and the regulatory landscape, which demand ethical guidelines in the developments and application of intracortical stimulators [61, 62]. This section discusses the ongoing technological and biological challenges related to the development of intracortical prostheses.

### 2.4.1. Resolution of artificial vision

To evoke phosphenes, short trains of charge-balanced biphasic pulses are often used [63]. The stimulation parameters are essential in defining characteristics of the phosphenes such as brightness, duration, size or colour [53]. However, the electrode impedance and placement may vary between patients [41], leading to threshold variation across patients, making comparing reported phosphene thresholds difficult.

Research shows that restoring a sizeable visual field is necessary to make artificial vision helpful in everyday life [53]. The visual field size is essential for interacting with the environment, as it affects one's understanding of the layout of space, depth perception and spatial cognition [64]. A sufficient spatial resolution, defined by the number of separable phosphenes in the visual field, is needed for a user to identify and recognise objects in the visual field. It has been estimated that at least 625 electrodes are required in a 1 cm by 1 cm area to produce a vision that allows for reading [65]. The projects discussed in section 2.3 meet this criterion; however, increasing the number of electrodes per area results in several challenges. For example, increasing the density of the electrodes per area increases the risk of cross-talk between the electrodes [38]. Another challenge is the possibility of incorrectly stimulating too many neurons, either causing the created phosphenes to fuse into a blob during synchronous activation of multiple electrodes [53] or activating interconnected neurons distant from the electrode [66]. Visual prostheses could, therefore, benefit from using current steering approaches that would limit the extent of the activated tissue during stimulation, reducing the risk of cross-talk and increasing the spatial selectivity [67, 68].

### 2.4.2. Image processing

Visual prostheses must perform two steps to convert the captured visual information into artificial vision. The first step concerns optimising visual information, whereas the second is about transforming this visual information into patterns of electrical stimulation [38]. Extracting useful features from a visual scene is a complex task, as is shown in Figure 2.6, because presenting a visual image to a user without accurate processing creates a crowded and confusing visual experience that offers insufficient guidance for navigating an unfamiliar environment [69]. The correct conversion of visual information into stimulation is essential as the visual field maps are patient-specific and can change over time [70, 71]. To accurately extract meaningful features, and to convert them into useful stimulation patterns, computer vision, machine learning, and psychophysics are required [38]. For example, machine-learning approaches could be applied to design electrical stimulation patterns that resemble those found in the brain [72].



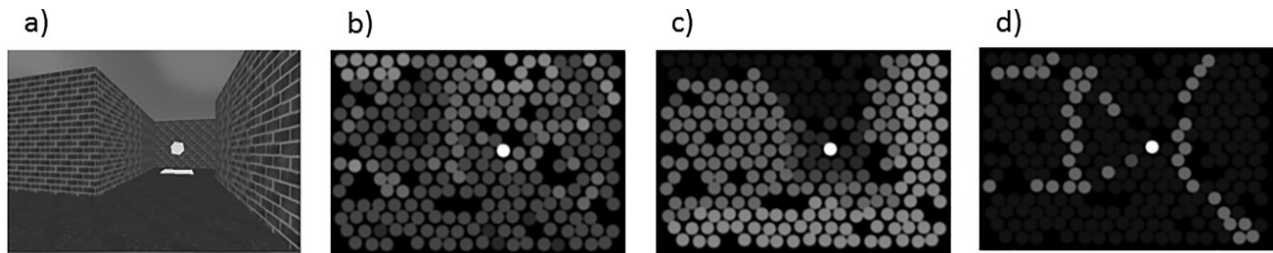


**Figure 2.6:** An illustration of simulated prosthetic vision renderings to explain the importance of extracting useful features from a visual scene. The actual image is shown in (a), where the next panels show images where the brightness of the original image (b), or the distance in the image (c), is matched to the brightness of the generated phosphenes. (d) shows what happens when the edges of the different surfaces of the environment are highlighted. Image is an adaptation of [69].

### 2.4.3. Wireless power and data transmission

The transfer of sufficient energy is a technological challenge in the design of intracortical prostheses. Neurostimulation is commonly applied with electrodes wired to an electric pulse generator [53]. While needed to connect the components, the presence of cables and connectors applies mechanical forces on the implant and the tissue, causing long-term scarring [73]. A different problem is the occurrence of fractures in the implanted wires, causing malfunctioning or non-functioning of the device [74]. To avoid these issues, wireless data and power transfer solutions can be used [73]. The use of inductive power transfer is the preferred solution for high-resolution intracortical stimulation due to the small distance between the transmitter and the receiver [60], as shown in Figure 2.7.

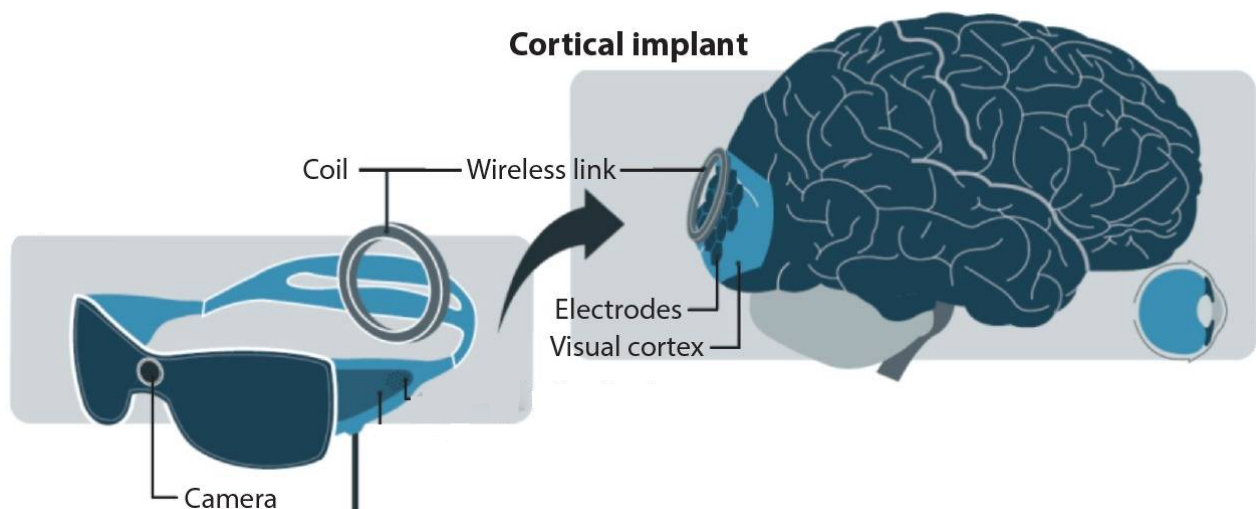


**Figure 2.7:** An illustration of an inductive link between the electrode tiles that are placed at the visual cortex and the glasses worn by the user, realising a small distance between the transmitting and receiving coils. Image is an adaptation of [75].

### 2.4.4. Long-term stability and biocompatibility

The use of intracortical electrodes triggers a response from the body. The insertion of electrodes into the tissue can lead to glial encapsulation, neuro-inflammatory responses or the loss of neuronal cells [27, 38, 76]. These responses, and the foreign body response, can cause complications and a reduction of stimulation efficiency [77, 78], therefore, the biocompatibility of the implanted materials is essential for long-term implantation in order to minimize the foreign body response [53]. Over the years, most implantable electrodes have been manufactured using silicone and platinum, which are well characterised in the context of implantation [79]. While not perfect, they enabled the testing of prostheses. However, developing new materials for electrodes with better biocompatibility has been ongoing, creating materials such as PEDOT:PSS and polystyrene sulfonate [80]. These materials have improved conductivity and impedance, improving the ability to monitor and generate neuronal activity.



### 2.4.5. Electrode Tissue Interface

When a metal electrode comes into contact with biological tissue, an interface forms that enables the exchange of electrical charges between the metal and its surroundings [81]. This Electrode-Tissue Interface (ETI) creates a highly non-linear charge transfer mechanism. However, it can be modelled by approximating the charge transfer [46, 82] as shown in Figure 2.8.

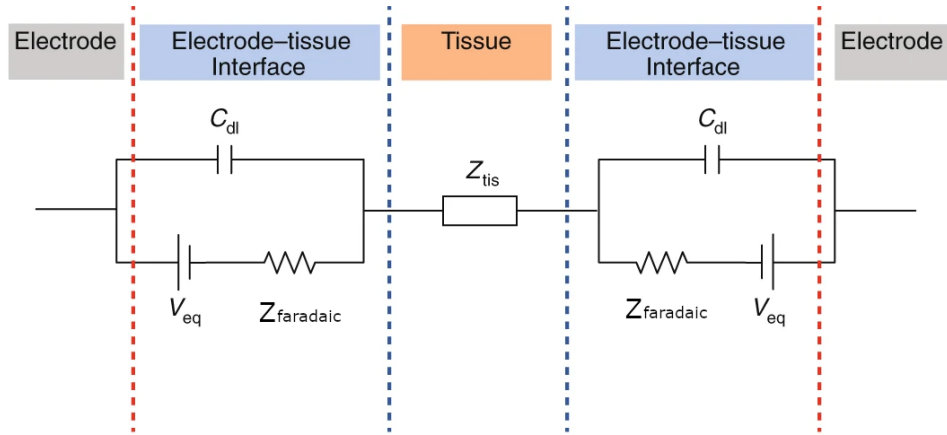


**Figure 2.8:** Electrical model of the electrode-tissue interface.  $Z_{tis}$  represents the tissue impedance where  $C_{dl}$  is the capacitive layer at the electrode-tissue interface. The chemical processes that can occur are modelled by  $Z_{faradaic}$ .  $V_{eq}$  models the electrochemical potential that acts as the driving force for the chemical processes. Image is an adaptation of [82].

The model explains the charged particles' reaction at the interface between the electrode and the surrounding neural tissue. The tissue resistance is modelled as  $Z_{tis}$ . Due to the separation of charge (electrons in the metal and ions in the tissue), an electrochemical double-layer  $C_{dl}$  is formed. The exchange of charge between the electrode and its surrounding tissue can cause non-reversible Faradaic reactions that can potentially cause damage to the tissue or the electrode. These reactions are modelled by the Faradaic impedance  $Z_{faradaic}$ . A voltage source  $V_{eq}$  is in series with this resistor, which models the electrochemical potential that acts as the driving force for chemical processes [82]. These faradaic reactions can create toxic byproducts or cause the electrochemical breakdown of water or other molecules in the tissue [27]. The material properties of the electrodes influence if and when these processes happen, affecting charge storage capacity and impedance. For example, increases in electrode material conductivity increase the charge transfer efficiency [80]. For the long-term safety of both the electrodes and surrounding tissue, the faradaic reactions should be minimised and proper modelling of the ETI could aid in achieving that goal [38].

## 2.5. Electrode design models and considerations

Researchers are improving and developing technologies to deal with the challenges explained in section 2.3. There is a need for a high-density, local stimulator combined with a reliable, long-term, stable tissue interface [53]. Progress in addressing these challenges has been slow, partly due to the high difficulty of experimental procedures used to validate the developed stimulating systems, typically requiring complex surgeries and experiments with primates and humans. The development of new electrode designs and stimulation paradigms, which could lead to an increased spatial density of phosphene generation and visual field coverage, is typically done without considering the resulting spatial extent of neuronal activation. Performing complex experiments for each new design is not a practical method, making the computational modelling of the electrode designs and stimulation paradigms essential. Researchers have created models to test their ideas without the need for complex experimental procedures. This section gives an overview of the different parameters that can be considered during an electrode's design and shows what models have been developed to model electrical activation and the influence of electrode parameters.

### 2.5.1. Considerations in electrode design

The most commonly used architecture types of intracortical electrode arrays are the Utah and Michigan type electrodes [83]. These architecture types are shown in Figure 2.9A. These shank-type electrodes apply stimulation using metal contacts placed along the shank's side or at the tip.

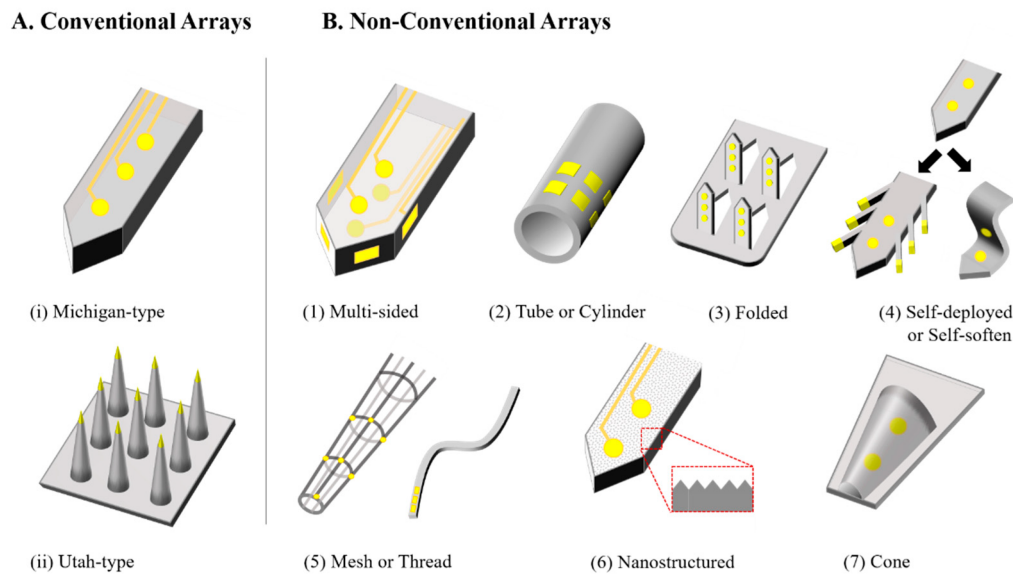


**Figure 2.9:** An illustration of conventional microelectrode arrays (a) and non-conventional microelectrode arrays (b). Image obtained from [83]

Various research groups have tried introducing unique features to conventional cortical arrays to overcome the challenges that traditional arrays could not resolve [83]. The considerations in electrode design are related to biological and technological aspects such as the electrode materials and the electrode geometry, which influences the electrode performance and energy consumption [38, 84]. The electrode fabrication process and used materials are essential for a reliable, safe, and long-term stable tissue interface [85]. The geometry of the electrode contacts can adjust the activated volume of neural tissue by increasing the localisation of delivered current [86, 87]. For example, a study comparing microelectrodes concluded that the current density on the surface of conical electrodes could be up to 10 times larger than the current density on similar size annular electrodes [88] and that choosing the most efficient electrode geometry to reduce power consumption depends on the distance from the target neurons to the electrode surface [88]. There is also the consideration of tissue damage that can result from the insertion of the electrodes; insertion likely damages neurons around the electrode [85], and after the insertion, glial scar forms around the electrode, influencing the behaviour of the stimulation [27].

### 2.5.2. Existing computational models for electrical stimulation

Various models have been developed to predict the effects of electrical stimulation, guiding researchers in optimising electrode designs and understanding the spatial distribution of electric fields in tissue [89]. These models have been developed over time, beginning with early studies by McNeal [90] and Rattay [50], which laid the foundation for understanding the general behaviour of nerve cells under the influence of electrical stimulation. However, as these models were purely analytical, solving such models took a lot of effort. The complexity, but also the ease of solving, increased with the introduction of Finite Element Modeling (FEM) [43], allowing observations about spike initiation to be explained that were based on geometric configurations using the AF. The strength of the application of FEM is shown in the versatility of computational models across various applications. For example, through FEM, it has been concluded that the orientation of an inductor coil greatly affects the strength of the induced electric field in intracochlear magnetic stimulation [91]. In this model, the induced electric fields are analysed as a function of inductor size, orientation and stimulation parameters. A different application is the investigation of the influence of voltage and current-controlled stimulation through models with different ETI interfaces for deep brain stimulation (DBS) electrodes [92].

Further advancements in the use of FEM led to reviews on modelling approaches [93] and the develop-

ment of biophysically realistic neuron models for simulating cortical stimulation [94]. While the model of [94] accurately describes the neuron's behaviour, it does not integrate the generated electric potential from a stimulating electrode. The reviews on modelling approaches discussed the pros and cons of applying certain boundary conditions in the model and how those conditions can affect the generated solution. The quality of FEM models have been updated through those discussions, but also due to new research. For example, by determining how boundary conditions must be implemented to represent metal stimulating electrodes appropriately [95]. Meanwhile, interactive visualisation tools emerged that could be used to analyse neuronal activity data in topological network models for rapid validation of simulation results [96].

Computational models extended to the analysis of the response of specific neuron types to electrical stimulation [72], the simulation of cortical circuits and those exploring the effect of cortical stimulation on the spiking probability of neurons in a volume of tissue [52]. While all these models are essential to improving the stimulation resolution, they do not look at the influence of the electrode geometry and electrode configurations and should combine their findings with the influence of such parameters to more accurately determine the reaction of tissue on extracellular stimulation. Some studies have focused on the impact of electrode geometries on the efficiency of neural stimulation and the variation of current density on the electrode surface [97], providing valuable insights for optimising electrode designs. However, as they only focussed on the influence of the electrode geometry on the current density, they did not look at the effect on the generated current density in the tissue. The described models in this section have allowed us to learn about aspects such as the response of different cell types, the influence of contact geometry on stimulation efficiency or how to accurately predict spatial regions of neuronal activation through electrode stimulation. However, there is still a lack of models that take the electrode geometry and configuration into account to determine their effect on aspects such as the spatial resolution of activated tissue to achieve higher-quality artificial vision.

## 2.6. Thesis objective

Based on the literature presented in this chapter, the author has defined that research is needed on the effect of different electrode geometries and electrode configurations on volumes of activated tissue to improve aspects of visual prostheses, such as resolution. While various models exist for specific simulations, such as those focusing on geometry or the effects of current steering, to the best of the author's knowledge, there is currently no available model or framework enabling users to conduct simulations assessing the combined effects of alterations in geometry and electrode configurations. This thesis aims to address a current gap in the literature by developing a framework that allows users to visualise the combined effects of alterations in electrode geometry and configurations.

# 3

## Method

To visualise the expected activated area due to extracellular current sources, a tool is created using Finite Element model (FEM) simulations. Using a parameterised model, VoNA (Visualisation of Neuronal Activation) visualises the anticipated spatial extent of neuronal activation. It offers the opportunity to visualise the effect of adjusting parameters such as the electrode configuration (monopolar, bipolar or multipolar), electrode contact spacing (pitch), electrode size (length & width), stimulation current or material properties. The first section provides a description of the model and the used settings. The second section describes the output of the model, whereas the last section discusses how the results will be evaluated.

### 3.1. Model description

As section 1.1.2 describes, different electrode configurations cause different results. For example, the size and shape of the stimulation region change with the configuration. Therefore, three distinct versions of the parameterised model were developed, each representing a different electrode configuration: monopolar, bipolar, and multipolar. Each model uses the Electric Currents interface of the AC/DC module of COMSOL Multiphysics 5.6 (COMSOL, Inc., Burlington, MA). This software package offers capabilities for simulating electric field distributions and can be used for stimulation in neuronal tissue models [49, 98]. To compare the results of the configurations fairly, each model is solved using the same settings. The settings used will be explained, but they can be adjusted in the tool by the user if required. An example of the parameterised model and the assigned material properties is shown in Figure 3.1 & Table 3.1.

The geometry used for all models consists of an intracortical micro-electrode positioned within the core of a uniform sphere of neuronal tissue where each configuration is designed to have one or more stimulation sites. This means that a monopolar configuration has one active contact, a bipolar configuration has two active contacts, and a multipolar configuration has more than two active contacts. In the used settings for solving the model, the electrode body is represented by a polyimide substrate with a conductivity of  $\sigma = 1\text{e-}12\text{ S/m}$  [78]. Its dimensions are  $100\text{ }\mu\text{m}$  long x  $90\text{ }\mu\text{m}$  wide x  $10\text{ }\mu\text{m}$  deep, and it is placed in the centre of a conductive sphere ( $800\text{ }\mu\text{m}$  radius). The sphere is modelled as a homogeneous and isotropic sphere of grey matter with a conductivity  $\sigma = 0.276\text{ S/m}$  [78, 94, 99, 100]. The electrode contacts are shaped as squares with rounded corners and are embedded flush with the surface. They are modelled as a homogeneous Platinum (Pt) body with  $\sigma = 8.9\text{e}6\text{ S/m}$  [78, 101]. Each electrode has an area of  $15\text{ mm}^2$  with a thickness of  $2\text{ }\mu\text{m}$  and is spaced  $9\text{ }\mu\text{m}$  apart centre-to-centre from any nearby placed contact. The corner radius of the electrodes is set to  $2\text{ mm}$  to avoid sharp corners (as well as mimic fabrication tolerances). Sharp corners can create singularities in the derivatives of the dependent variables that COMSOL uses [102]. The dimensions of the contact and body, as well as the materials and their properties, are consistent with the dimensions of electrodes that have been designed for intracortical stimulation [27, 78, 103].

To solve the parameterised models, quasi-static conditions have been assumed [93], neglecting transients at the start and end of the current pulse and using an isotropic extracellular medium. Dirichlet boundary conditions have been applied by grounding the outermost layers of the sphere. Inactive electrodes are left floating to match the findings from literature [95]. The electrode contacts have been implemented as boundary current sources using the dimensions above. This simulates the application of current mode stimulation (CMS) [46]. It is the favoured method due to its control over the injected charge into the tissue [29]. A DC current is used

to compare the results across the resistive tissue even though phosphenes in the visual cortex are typically generated using pulses that range from 75 to 200 Hz [104]. This reduces the comparison's dimensionality by removing the electrode's capacitance from the results [88].

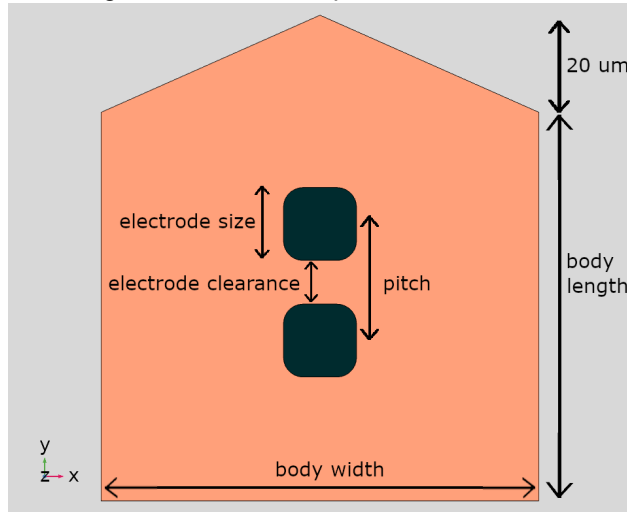


**Figure 3.1:** Example of the parameterised finite element model. Showing the electrode substrate (orange) with two contacts (black) in a homogeneous sphere (grey).

Parameters	Value [Unit]
Body length	80 [μm]
Body width	90 [μm]
Electrode size	15 [μm]
Electrode clearance	9 [μm]
Electrode pitch	size + clearance [μm]
Tissue conductance	$\sigma = 0.276$ [S/m]
Tissue permittivity	$\epsilon_r = 88.9$
Substrate conductance	$\sigma = 1e-12$ [S/m]
Substrate permittivity	$\epsilon_r = 11.7$
Contact conductance	$\sigma = 8.9e6$ [S/m]
Contact permittivity	$\epsilon_r = 1$

**Table 3.1:** Material properties & parameters of the model.

The default mesh that COMSOL applies is a tetrahedral mesh which reduces the computational load due to its simplicity and can be used due to the non-complex structures present in the model. The quality of the results has been generated for several element sizes and is used to determine the mesh quality through an iteration among the different element sizes to determine when the peak potential at the desired location changed by  $< 2\%$  and the activation threshold adjusted by 1 %. The result is a mesh domain consisting of 525532 elements.

## 3.2. Model output

Solving the model starts by solving for the generated electric potential. The physics used in the Electric Currents interface of the module uses Poisson's equation, which relates potential and charge density, as a partial differential equation (PDE) to solve the electrostatic fields [105]. The following relations are used to derive Poisson's equation. From Maxwell's equations, the differential form of Gauss's law is shown in Equation 3.1. Using the definition of the electric field as shown in Equation 3.2, the first equation can be rewritten to form Equation 3.3, known as the Poisson's equation. In these equations,  $\nabla$  represents the laplacian of the scalar function  $V$ , which is the electric potential.  $\mathbf{E}$  represents the electric field,  $\rho_v$  the volume charge density and  $\epsilon$  the permittivity of the medium.

$$\nabla \cdot \mathbf{E} = \frac{\rho_v}{\epsilon} \quad (3.1)$$

$$\mathbf{E} = -\nabla V \quad (3.2)$$

$$\nabla^2 V = -\frac{\rho_v}{\epsilon} \quad (3.3)$$

Two assumptions concerning the medium are made during the model setup. The first assumption is that brain tissue can be modelled as homogeneous and isotropic [95]. The second is that only charge is present due to the applied current on the active electrode contacts, meaning no external charges are present. The assumptions create a linear scaling concerning the generated voltage, allowing us to use the principle of superposition.

The output of the solved models is formed by applying a current to the active contact in the respective model configuration. This means that the active electrode contact acts as a current source or sink, and non-active electrodes have been set to generate no current. The model's results show an example of linear scaling when applying a current magnitude of  $\pm 10 \mu\text{A}$ . Changing this value, e.g. reducing it by half to  $\pm 5 \mu\text{A}$ , would

produce voltages that are 0.5 times lower. The currents mentioned are in the typical values range ( 5 to 80  $\mu\text{A}$ ) for intracortical microstimulation [36, 38].

Evaluation of the results is done at selected electrode-axon distances. Since the tool is a parameterised model, all mentioned parameters can be changed if needed. In this way, the tool creates the opportunity to visualise the effect of adjusting parameters such as the electrode configuration or contact spacing (pitch). An example of the results obtained from using a set of standard settings (applying an electric current of  $\pm 10 \mu\text{A}$ ) is shown in Figure 3.2 with an example axon centred over the electrode contacts.

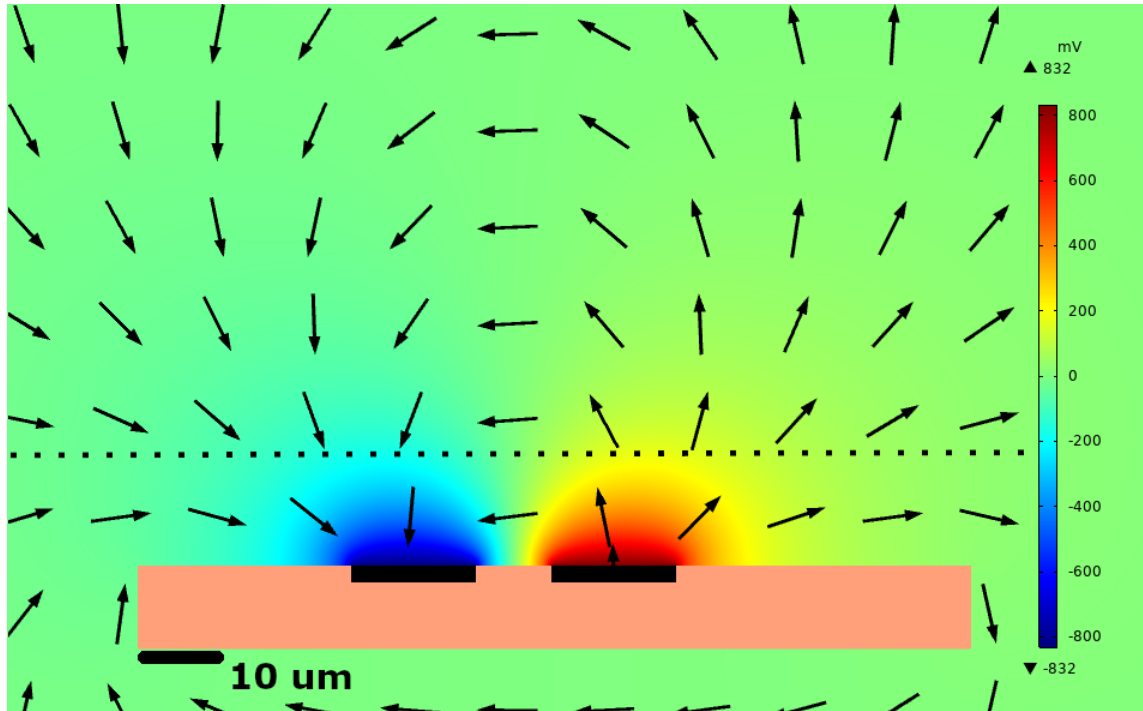


**Figure 3.2:** Distribution of potential for a bipolar electrode configuration. The outer boundary of the sphere is set to ground. The black arrows show the direction of the current (current of  $\pm 10 \mu\text{A}$ ). The dashed horizontal line indicates the position of an axon at  $15 \mu\text{m}$  from the electrode

### 3.3. Evaluation of the spatial extent of stimulation

The results from the solved model are assessed using two different methods to determine the volume of activated tissue. The first method to evaluate the region of activated tissue is observing the generated current density. The current density forms an indication of effective current spread in the medium. This effective current spread visualises a volume where neuronal activation is possible. By combining the formula for current density ( $J = \frac{I}{A}$ ) with the current-distance relation from subsection 2.2.1 ( $I = Kr^2$ ), assuming the surface of a sphere, the minimal required surface current density can be expressed as Equation 3.4.

$$J = \frac{K}{4\pi} [A/m^2] \quad (3.4)$$

This current density threshold differs for the used medium. For cortical tissue, this threshold is  $675 \mu\text{A}/\text{mm}^2$  [17] and exceeding this will create a region where neurons are assumed to be stimulated [26].

The second method to assess the probability of stimulation is the Activating Function (AF). The AF uses the spatial derivative of the electric potential along a nerve. It determines whether depolarisation is present that surpasses the required threshold to trigger an action potential [50]. The most considerable excitation occurs where the largest gradient along the neuronal structures is found. The AF can be interpreted as a virtual current injected near the axon or node of Ranvier. A positive current tends to create depolarisation, whereas a negative current tends to create hyperpolarisation. When the virtual current exceeds the threshold, nerves will be activated due to depolarisation [43]. A simplified version of the AF is shown in Equation 3.5 and more details about the AF can be found in subsection 2.2.2.

$$f_n = \frac{d}{4c \cdot \rho_i} \cdot \frac{V_e^2}{dx^2} \quad [\mu A/mm^2] \quad (3.5)$$

The threshold for activation using the AF depends on the properties of the neuron. The activation of myelinated neurons is found to have a threshold of  $3 A/m^2$  [52]. Non-myelinated axons have a threshold of  $60 A/m^2$  [52]. An example plot of the AF is shown in Figure 3.3, showing a plane where the AF reaches values equal to or larger than the threshold for neuronal segments with a horizontal orientation (along the x-axis). The plot shows a xy-plane at  $z = 15 \mu m$  and highlights possible activation areas around the electrode for a horizontal observation direction. Changing the observation direction will show different results. This plot assumes the following values about the membrane:  $c_m = 1 \mu F/cm^2$ ,  $\rho_i = 300 \Omega \cdot cm$  and  $d = 10 \mu m$ .

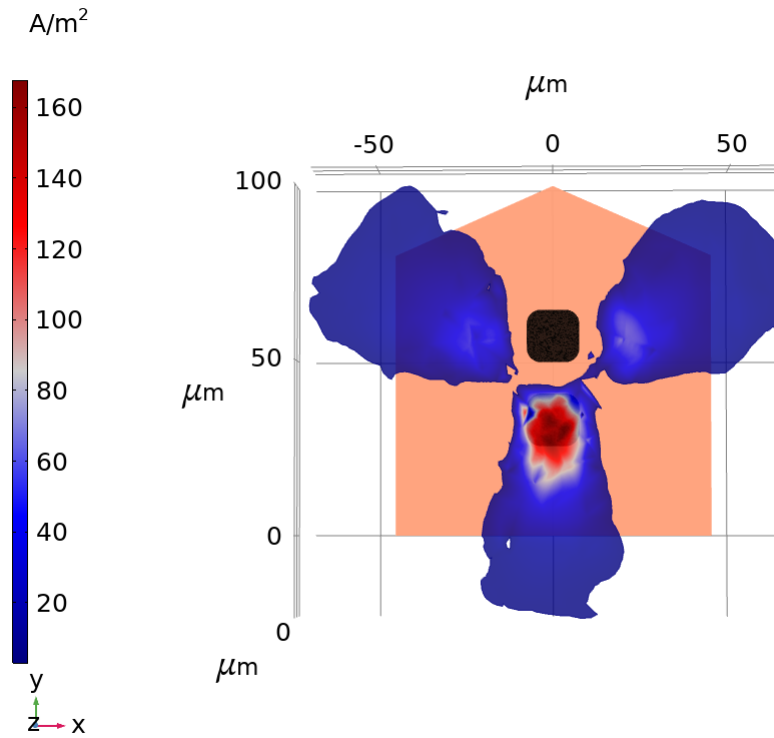


**Figure 3.3:** Plot showing the resulting activating function (AF) for neurons orientated in a horizontal observation direction (the x-axis) for a bipolar electrode configuration. The results show an xy-plane for  $z = 15 \mu m$  and are created using a current amplitude of  $10 \mu A$ . The AF is plotted using a threshold of  $3 pA/\mu m^2$  and assumes the following values about the membrane:  $c_m = 1 \mu F/cm^2$ ,  $\rho_i = 300 \Omega \cdot cm$  and  $d = 10 \mu m$ .

# 4

## Results

### 4.1. VoNA: the Visualisation of Neuronal Activation

Chapter 3 provided an overview of the model setup and output of the developed tool. VoNA is exported as a COMSOL application and allows users the flexibility to make edits if necessary. Both the application files and the model files are publicly accessible on GitHub.

VoNA is designed to follow an intuitive workflow to obtain the desired results. This workflow consists of five steps, each with its corresponding section. The initial step requires the user to define the properties and dimensions of the model. For example, the material conductivities, electrode dimensions or the applied stimulation current magnitude. With the material properties and model dimensions specified, step 2 concerns constructing the model's geometry. The model is built in this step and can be inspected to see if it matches the required settings. Steps 1 and 2 and their required entries are shown in Figure 4.1.

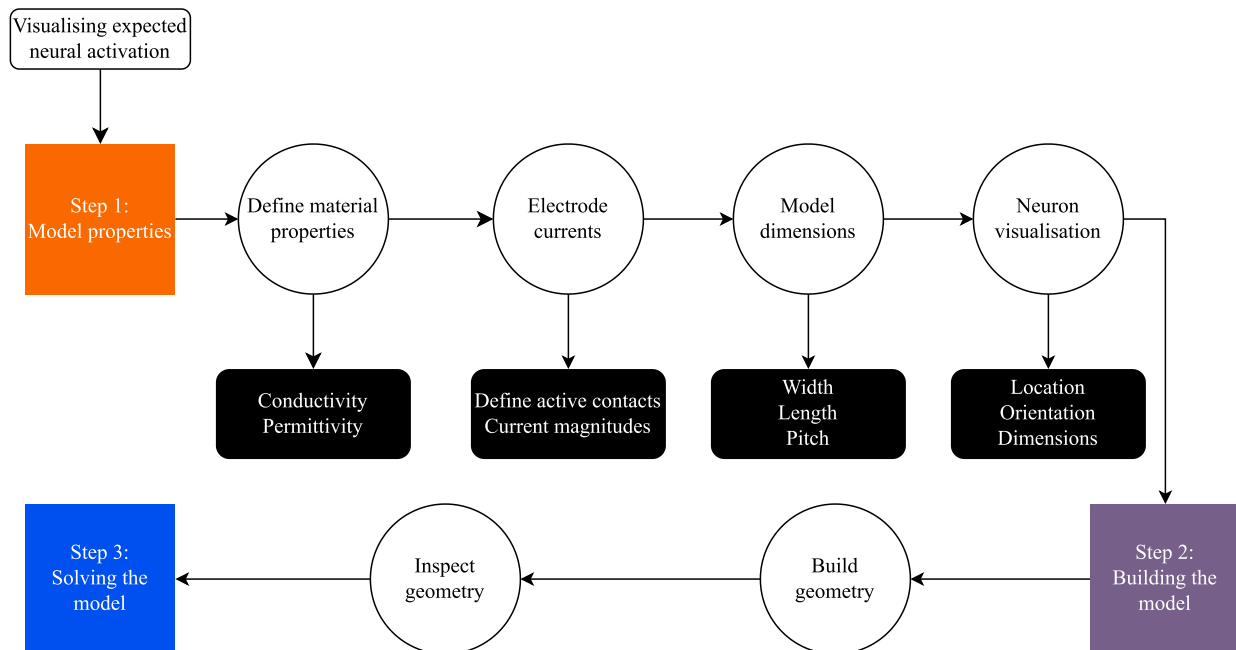


**Figure 4.1:** A flowchart explaining the first two steps of the workflow on how to use VoNA. It concerns itself with defining the model properties and building the geometry.

If the geometry is satisfactory, step 3 involves selecting the parameters to be swept and then computing the solution. Upon completion of the computation, step 4 allows the user to select and fine-tune the required data by defining plot conditions. For example, setting threshold values or defining solution datasets. Users can generate and visualise the desired plots when suitable conditions are applied in step 5. Steps 3 - 5 and their entries are shown in Figure 4.2.



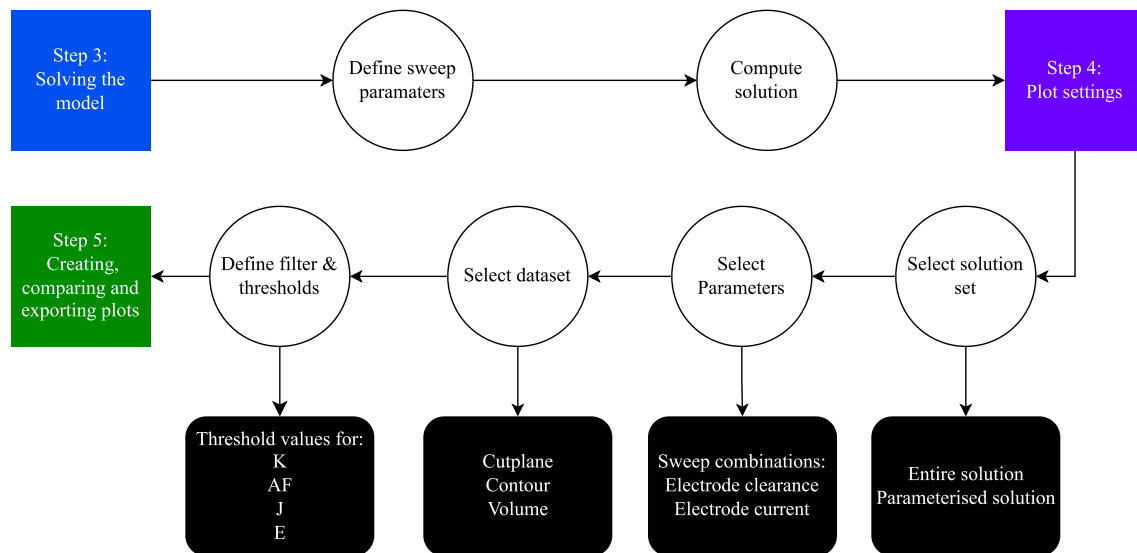
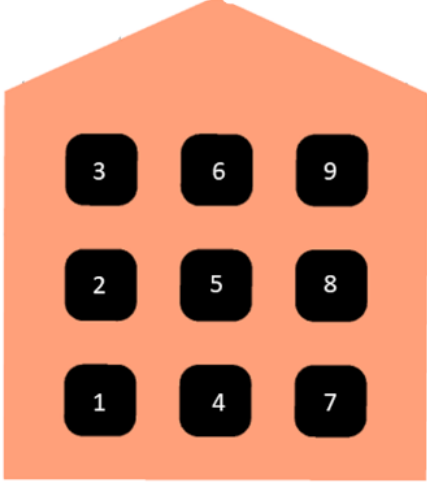


**Figure 4.2:** A flowchart explaining steps 3 - 5 on how to use VoNA. It shows when to compute the solution, what options are concerning data selection and when the plots can be generated.

A more in-depth view of the parameters that must be set in step 1 is shown in Figure 4.3. In this step, the material properties of the model have to be defined by providing the material conductivity and its relative permittivity. At this moment, changing the dimensions of the electrode body and contacts is possible. The image explains the numbering used in the tool concerning the electrode contacts. This gives the user the ability to control the current of each contact. Setting the current to 0 A indicates a floating contact. Steps 2 and 3 require using the buttons in the ribbon at the top of the tool. There, buttons can be found to build the geometry or compute the solution.

▼ Material properties		
Pt_conductivity:	8.9e6	S/m
Pt_Er:	1	
Poly_conductivity:	1e-12	S/m
Poly_Er:	11.7	
Tissue_conductivity:	0.276	S/m
Tissue_Er:	88.9	
▼ Electrode current		
positive_electrode_current:	10	uA
negative_electrode_current:	-10	uA
▼ Electrode contact and body properties		
electrode_size:	15	um
electrode_clearance:	12	um
electrode_depth:	2	um
body_width:	88	um
body_length:	80	um
▼ AF information input		
axon_diameter:	10	um
axoplasm_resistivity:	300	ohm-cm
▼ Neuron visualisation input		
neuron_x:	-50	um
neuron_y:	middle_between	m
neuron_z:	15	um
neuron_radius:	2	um
neuron_length:	100	um



▼ Current definition for each electrode contact		
Current of contact 1	positive_electrode_current	A
Current of contact 2	negative_electrode_current	A
Current of contact 3	positive_electrode_current	A
Current of contact 4	negative_electrode_current	A
Current of contact 5	positive_electrode_current	A

**Figure 4.3:** Step 1: Model properties. In this step, the user has to define material properties, dimensions and active electrode currents.

In step 4, the required images' plot settings must be defined. This includes defining the use of a dataset. The dataset can contain the solution of a parametric sweep or just a part of the entire solution. The user must also define what part of the solution shall be plotted. For example, to plot the data of XY-plane at a specific z coordinate or to show a volume plot of the entire solution. A list of options for the plot settings is presented in Figure 4.4.

Dataset: Study 1/Parametric Solutions (sol15)

Dataset: Study 1/Adaptive Mesh Refinement Solutions 1 (sol12)

Parameter value (electrode\_clearance (um)): 9

Parameter value (positive\_electrode\_current (uA),...): 3: positive\_electrode\_current=10 uA, negative\_electrode\_current=-10 uA

select what data you want to view: cutplane XY z = 15[um]

select the view of your data: standard view -2

Threshold definitions

excitability_constant_1:	675	uA/mm <sup>2</sup>
excitability_constant_2:	1292	uA/mm <sup>2</sup>
F_threshold_myelinated:	3	pA/um <sup>2</sup>
F_threshold_non_myelinated:	60	pA/um <sup>2</sup>

**Figure 4.4:** Step 4: Plot settings. In this step, the user has to define the plot conditions. E.g., defining the solution set (with or without sweep results), showing the results in a 2D plane or as a 3D volume, specifying thresholds, and filtering the results if needed.

To give the reader an example of the contents of VoNA, Figure 4.5 shows a preview.

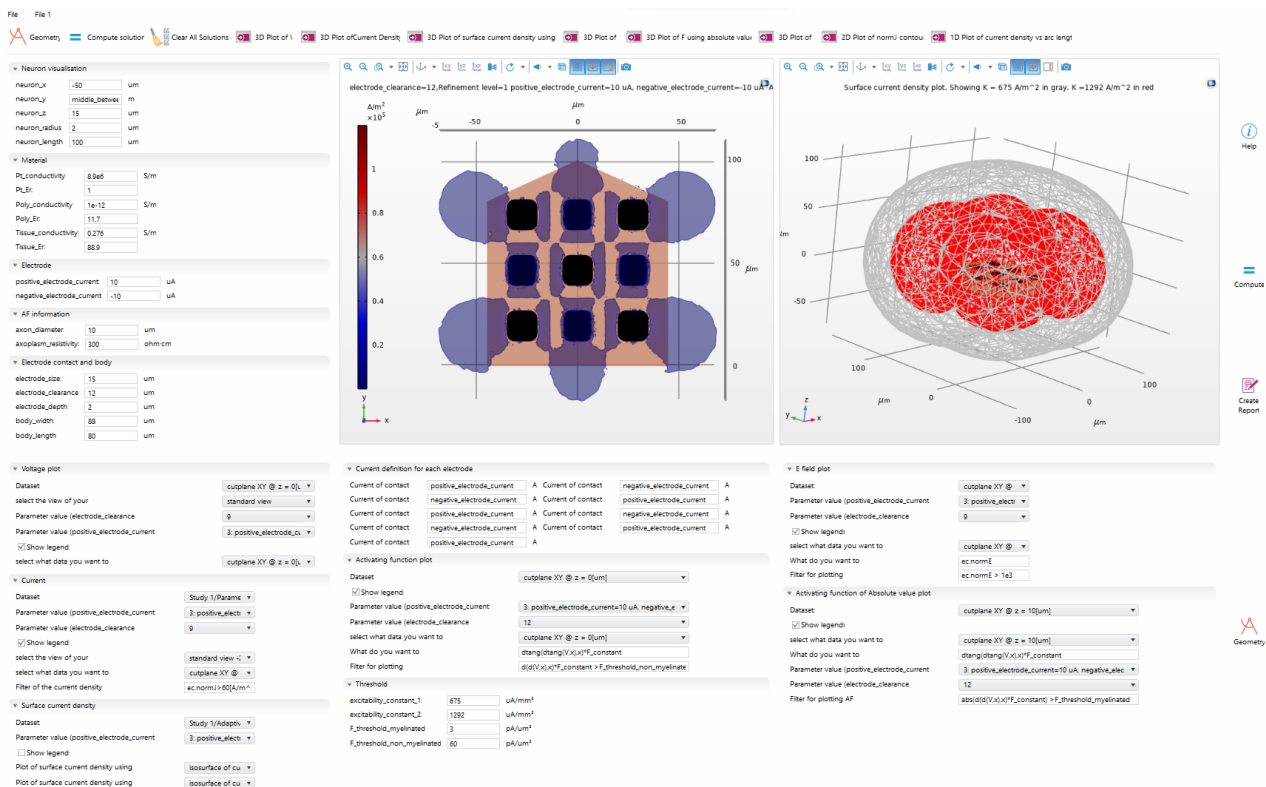


**Figure 4.5:** A preview of VoNA.

An overview of the workflow described is outlined in Figure 4.6.

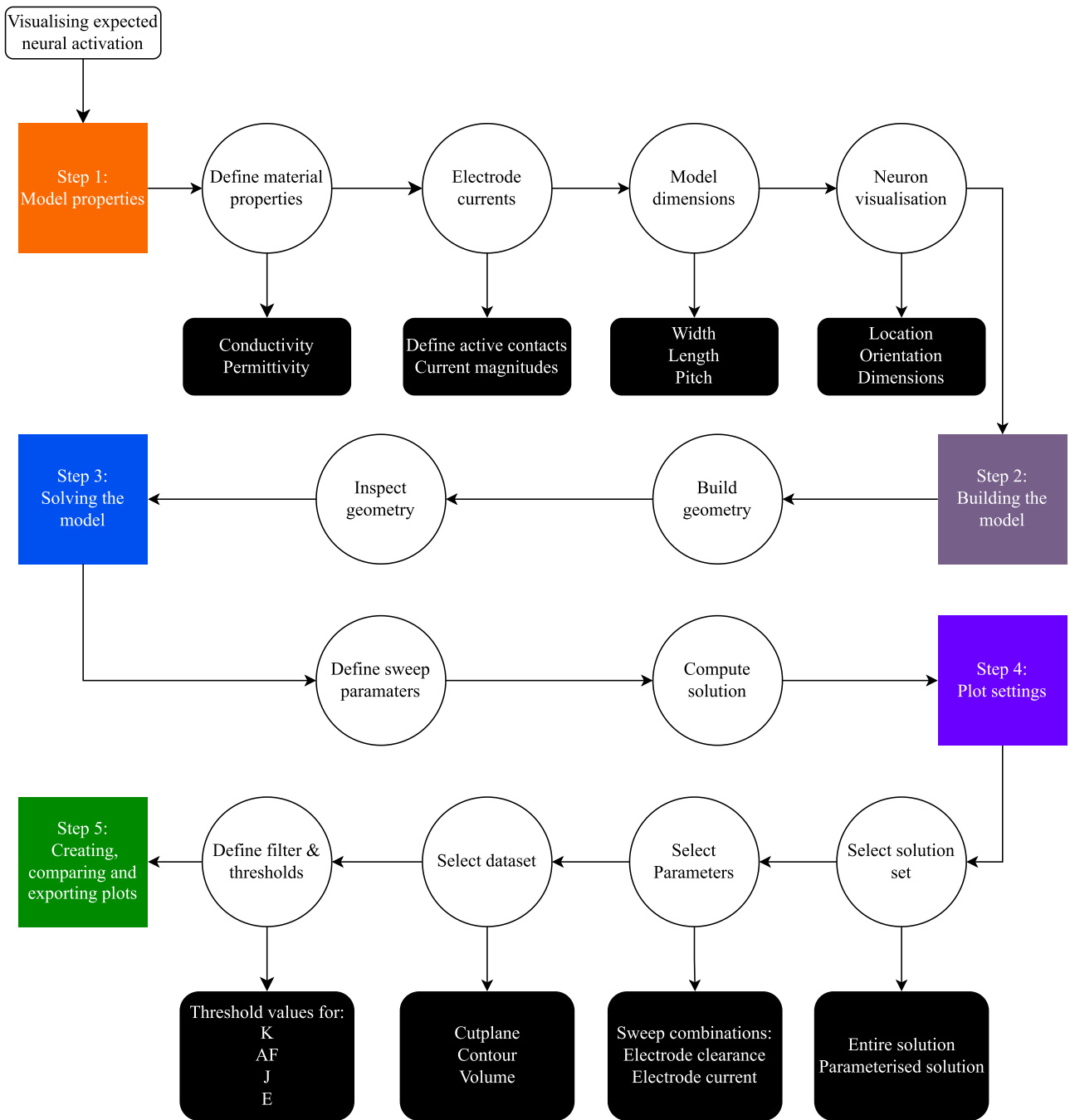


**Figure 4.6:** A flowchart of the operating steps on how to use VoNA.

As described in section 3.1, the model is parameterised, focusing on the accessibility of results across various scenarios. The selected parameters offer numerous options for adjustment. For example, the choice of stimulation configuration (monopolar, bipolar, or multipolar), adjustment of electrode contact spacing (pitch), customisation of electrode size (length and width), and modulation of stimulation current. Additionally, users can modify material properties or include a simplified neuron (represented as a cylinder) for visualisation purposes. The simplified neuron can be used as a point of reference.

Due to the available options that can be changed in the model, this results section aims to highlight the significance of adjusting these parameters. It is then up to the user to adjust the settings towards their specific needs and explore the possibilities. Some examples best illustrate the strengths and capabilities of the designed tool. The following sections will explore the effects of modifying the described parameters. For example, the effect on the generated potential, current density, electric field and activating function. Each

presented example uses the settings stated in Table 3.1 unless mentioned otherwise.

## 4.2. Observing the generated electric potential

The generated electric potential is a reference for observing the expected spatial stimulation due to the relations described in section 3.2. Analysing the electric potential provides insights into whether the modified parameter yields the desired effect.

A notable difference in generated electric potential can be observed by comparing the different electrode configurations. This is shown in Figure 4.7. Each sub-image shows the electric potential created by one of three electrode configurations. The electric potential is shown on a 2D xy-plane at a distance of  $15 \mu\text{m}$  from the electrode surface and is created by applying a current magnitude of  $\pm 10 \mu\text{A}$ . Figure 4.7a shows a uniform electric potential that decreases radially outwards from the electrode. This behaviour of a monopolar electrode configuration is explained by modelling the electrode configuration as a point source, which electric potential is described by Equation 4.1.

$$V = \frac{q}{4\pi\epsilon R} \quad [V] \quad (4.1)$$

Comparing the generated electric potential of the monopolar configuration to the bipolar electrode configuration (Figure 4.7b) shows a clear difference. The bipolar electrode configuration can be modelled as an electric dipole. While the generated electric potential is similar to the monopolar electrode, it is more confined in space. The produced potential falls off much faster. This behaviour can be seen more clearly by looking at Figure 4.8. The image shows the decrease of the generated electric potential of the bipolar configuration as a function of  $z$ , the distance away from the electrode surface. It shows that the electric potential is falling off radially with a factor  $r^2$  as is described by Equation 4.2.

$$V = \frac{q d \cos(\theta)}{4\pi\epsilon R^2} \quad [V] \quad (4.2)$$

The multi-polar configuration shown in Figure 4.7c shows similar results to the bipolar configuration, but is even more confined in certain directions. This can be explained by the two electrode contact pairs used. The electrode contacts are numbered in Figure 4.3. The contact pairs, 2,8 for the negative current and 4,6 for the positive are equal in strength, creating an even more confined dipole-like electric potential. Changing the active electrodes' magnitude, number, and location will change the produced output. It provides a demonstration of the options that are available while using the multi-polar stimulation configuration.

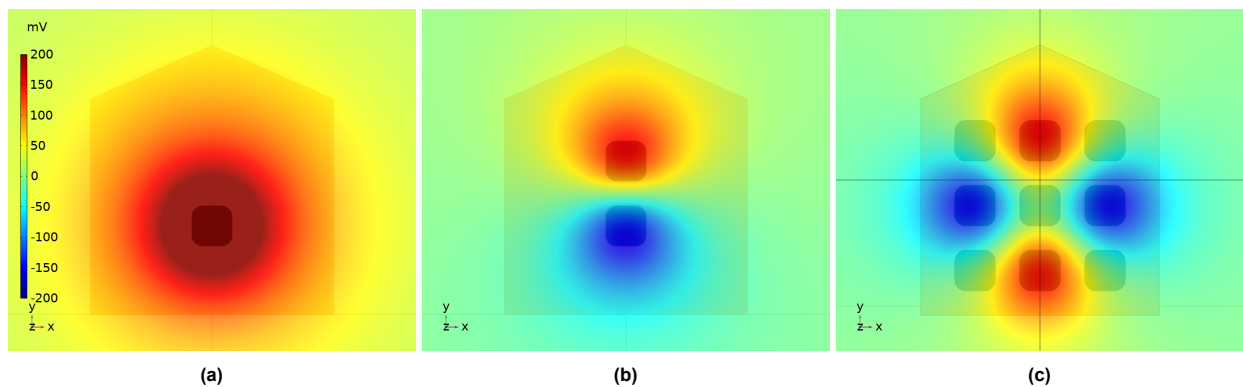


**Figure 4.7:** Electric potential generated by different electrode configurations at an XY-plane for  $z = 15 \mu\text{m}$ . It shows the results for a monopolar (a), bipolar (b) and multipolar (c) simulation in the subplots. The contact pairs of the multipolar configuration are 2,8 for the negative current and 4,6 for the positive. Each image uses the same colour range as defined in the legend of the monopolar image. Its range has been set to show values from -200 to +200 mV.

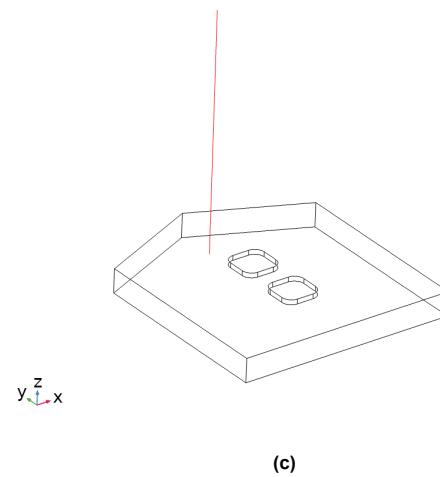
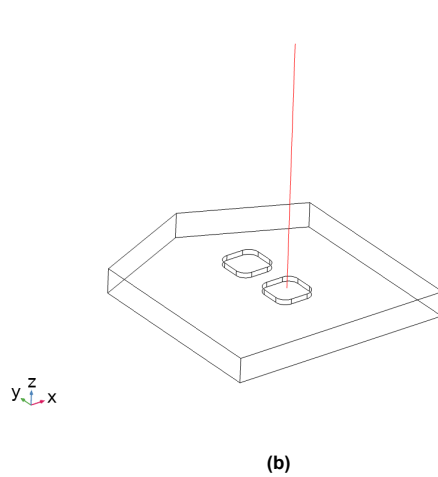
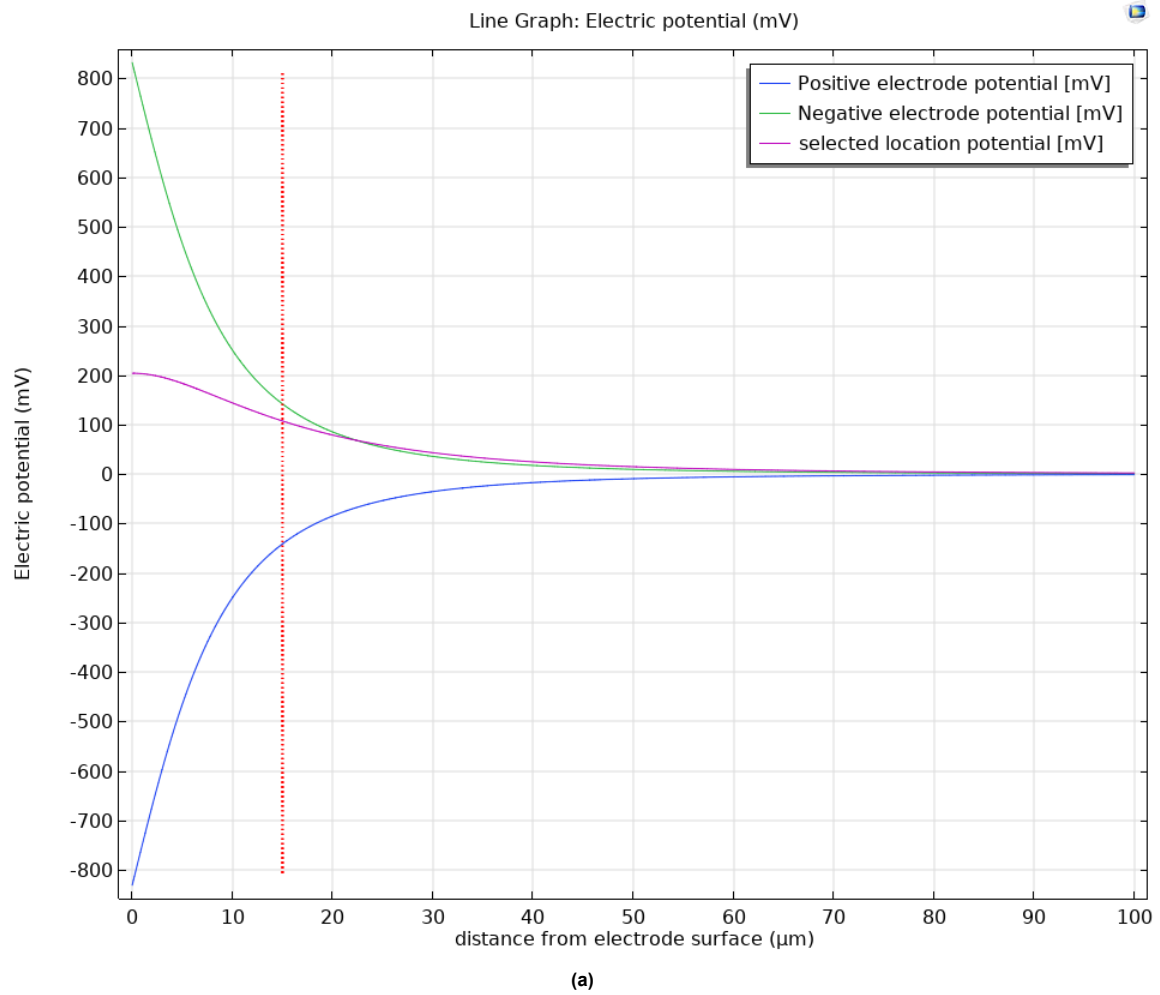


**Figure 4.8:** The electric potential as a function of distance from the electrode surface in the positive  $z$  direction. The dotted line represents a distance of  $z = 15 \mu\text{m}$ . The blue and green lines plot the electric potential at the location of a positive and negative electrode, respectively, as shown in (b). The purple line shows the electric potential for the location indicated in (c).

### 4.3. Influence of the electrode contact pitch

The effect of changing the distance between the electrode contacts is shown in Figure 4.9. It shows that when multiple sources are present, they will interact with each other. Each electrode contact contributes towards the generated voltage according to the principle of superposition. The applied current for each contact in the bipolar electrode configuration example is equal in strength but opposite in polarity. The opposites interact with each other, reaching a balance in between the two contacts. Increasing the distance between the contacts reduces their mutual influence, reducing the area of balancing and increasing the area of their respective applied electric potential. This is seen when you compare Figure 4.9a and Figure 4.9c. Similar behaviour is observed in the multipolar configuration; however, the behaviour depends on the number of active electrodes used and the magnitude of the applied current.

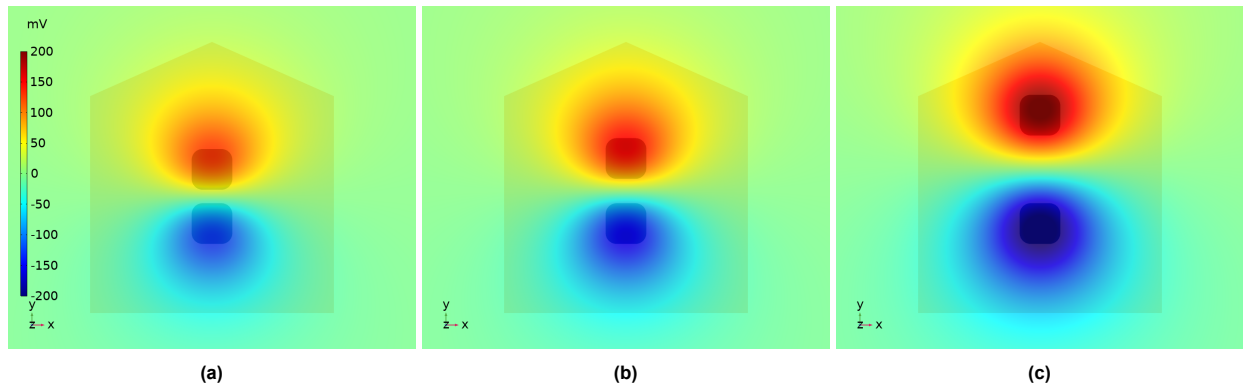


**Figure 4.9:** Potential generated by bipolar electrode configuration for a pitch of  $5\mu\text{m}$  (a),  $9\mu\text{m}$  (b) and  $25\mu\text{m}$  (c) at a XY-plane for  $z = 15\mu\text{m}$  above the contacts. Each image uses the same colour legend range.

### 4.4. Electric fields and their gradients

The electric field is calculated as a function of potential as explained in section 3.2. The electric field is mathematically expressed as  $\mathbf{E} = -\nabla V$ . Therefore, the principles that hold for the generated potential also apply to the electric field.

In COMSOL, the magnitude of the electric field is referred to as normE, defined by Equation 4.3. Figure 4.10 shows an example of the electric field amplitude for three different electrode configurations.

$$||E|| = \sqrt{(E_x^2 + E_y^2 + E_z^2)} \quad [V/m] \quad (4.3)$$

The results have been filtered to show only regions where the electric field strength exceeds  $1\text{ kV/m}$  to highlight differences between the electrode configurations. This threshold was chosen for its effectiveness in highlighting distinctions between the setups, though it holds no specific relevance to the expected area of neuronal activation.

The electric field displays a uniform gradient in all directions for the monopolar configuration (Figure 4.10a). This consistent gradient changes in the presence of additional active electrode contacts. The additional contacts interact, creating a non-spherical spread. This non-spherical spread introduces a gradient within the electric field that varies depending on the direction of observation and the arrangement of contacts.

The impact of observation direction is illustrated in Figure 4.11. It shows the electric field components in a multipolar configuration electrode's  $x$ ,  $y$ , and  $z$  directions. Each element possesses similar field strength but applies this strength in distinct ways. While the covered area is comparable for  $E_x$  and  $E_y$ , it differs from  $E_z$ . This characteristic can be used to experiment with the multipolar electrode configuration, aiming to establish a specific gradient in targeted regions. For instance, amplifying the electric field gradient in certain directions to stimulate specific neurons while avoiding or reducing stimulation in other directions. A few examples are shown in Figure 4.10. It shows three different multipolar electrode contact configurations and their resulting fields. By using different electrode contacts and varying the pattern of active contacts, the images show that the obtained fields also differ, proving the benefits of applying the concept of current steering.

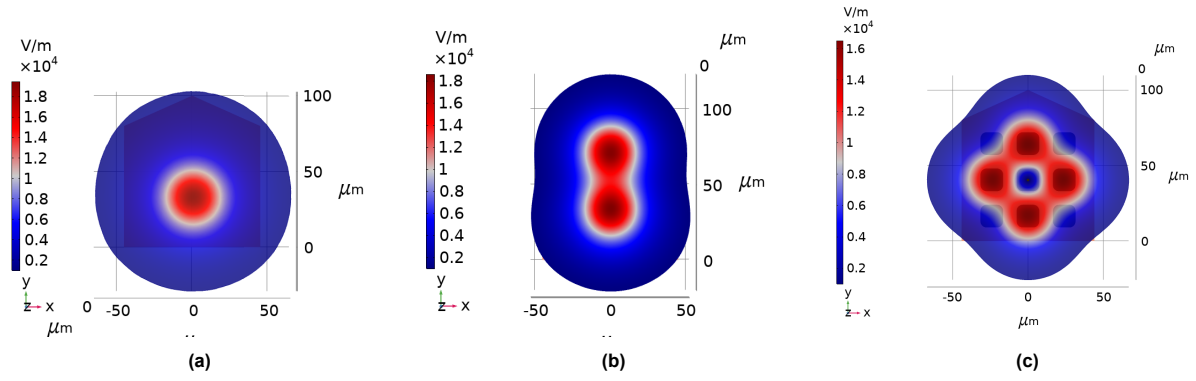


**Figure 4.10:** Electric field magnitude illustrated for a monopolar (a), bipolar (b) and multipolar (c) electrode contact configurations on an XY-plane for  $z = 15 \mu\text{m}$ . The contact pairs of the multipolar configuration are 2,8 for the negative current and 4,6 for the positive. To highlight the differences between the configurations, the results have been filtered to show only electric field strengths that exceed 1 kV/m.

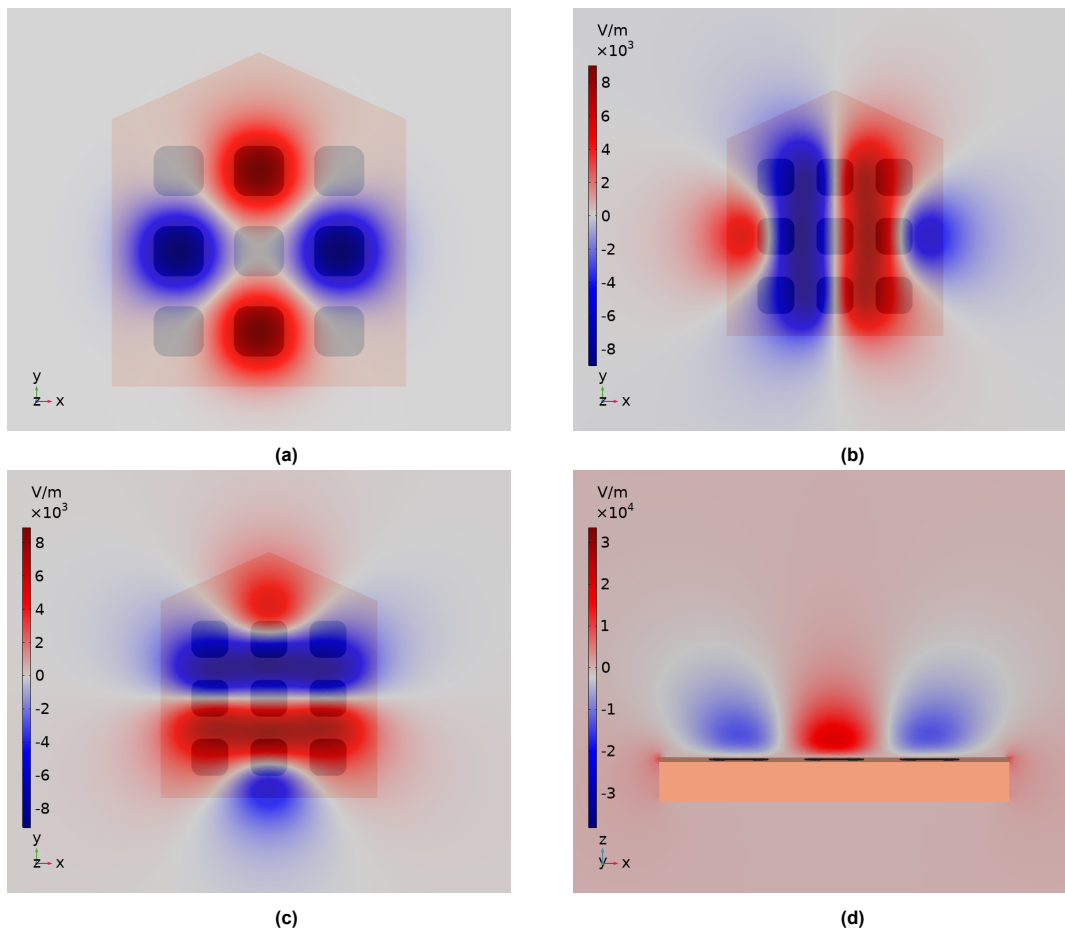


**Figure 4.11:** Comparison of the electric field for a multipolar electrode configuration in three directions. The contact pairs of the multipolar configuration, shown in (a), of the multipolar configuration are 2,8 for the negative current (shown in blue) and 4,6 for the positive (shown in red). (b) and (c) show the electric field gradients  $E_x$  and  $E_y$  at a XY-plane for  $z = 15 \mu\text{m}$ . The distribution of  $E_z$  is shown for a ZX-plane at  $y = 0 \mu\text{m}$ .



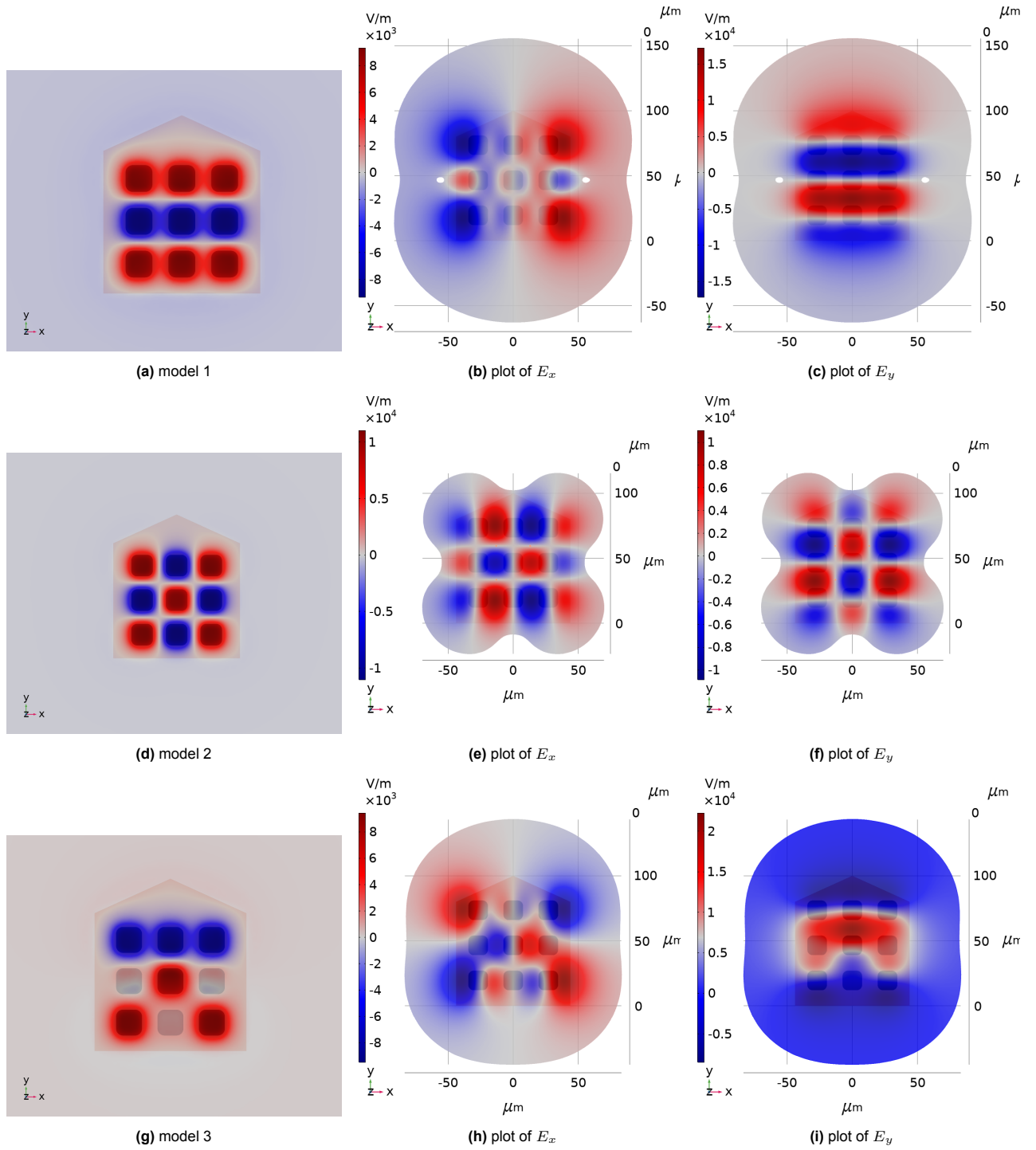


**Figure 4.12:** Electric field component in x and y direction for three different multipolar electrode configurations 15  $\mu\text{m}$  above the electrode contacts. These images have been made using the models shown in the left column, where each contact has the same current magnitude. Positive contacts are shown in red. Negative contacts in blue. To highlight the differences, a filter of 1 kV/m has been applied.



## 4.5. Estimating neuronal activation using surface current density

The current required to activate a neuron is determined by the distance between the neuron and the electrode contact, as explained in subsection 2.2.1. The effective current spread from an electrode contact can be expressed as Equation 4.4, where  $I$  represents the applied current magnitude in  $[\mu A]$ ,  $r$  denotes the current spread in  $[mm]$ , and  $K$  stands for the excitability constant  $[\mu A/mm^2]$ .

$$r = \sqrt{\frac{I}{K}} \quad [mm] \quad (4.4)$$

The model can compute the surface current density necessary for inducing neuronal activation using the constant  $K$  and the applied electrode current. The minimal required surface current density can be expressed as Equation 4.5.

$$J = \frac{K}{4\pi} [A/m^2] \quad (4.5)$$

Using the minimal required surface current density, an area is plotted in Figure 4.13 to indicate where neurons are likely to be stimulated. The image shows the results for three different electrode contact configurations. Each subimage illustrates the effective current spread spread for  $K = 675 \mu A/mm^2$  (gray) and  $1292 \mu A/mm^2$  (red). Comparing the configurations reveals variations in both shapes and the total covered area. As observed in section 4.2, each contact contributes uniquely, influencing the generated surface current density. This effect becomes more pronounced when altering the applied contact currents, shown in Figure 4.14. The shape and covered area vary significantly by changing the applied contact currents while keeping the same active contacts. Further research into current steering through electrode contact configurations or contact currents may yield untapped benefits.

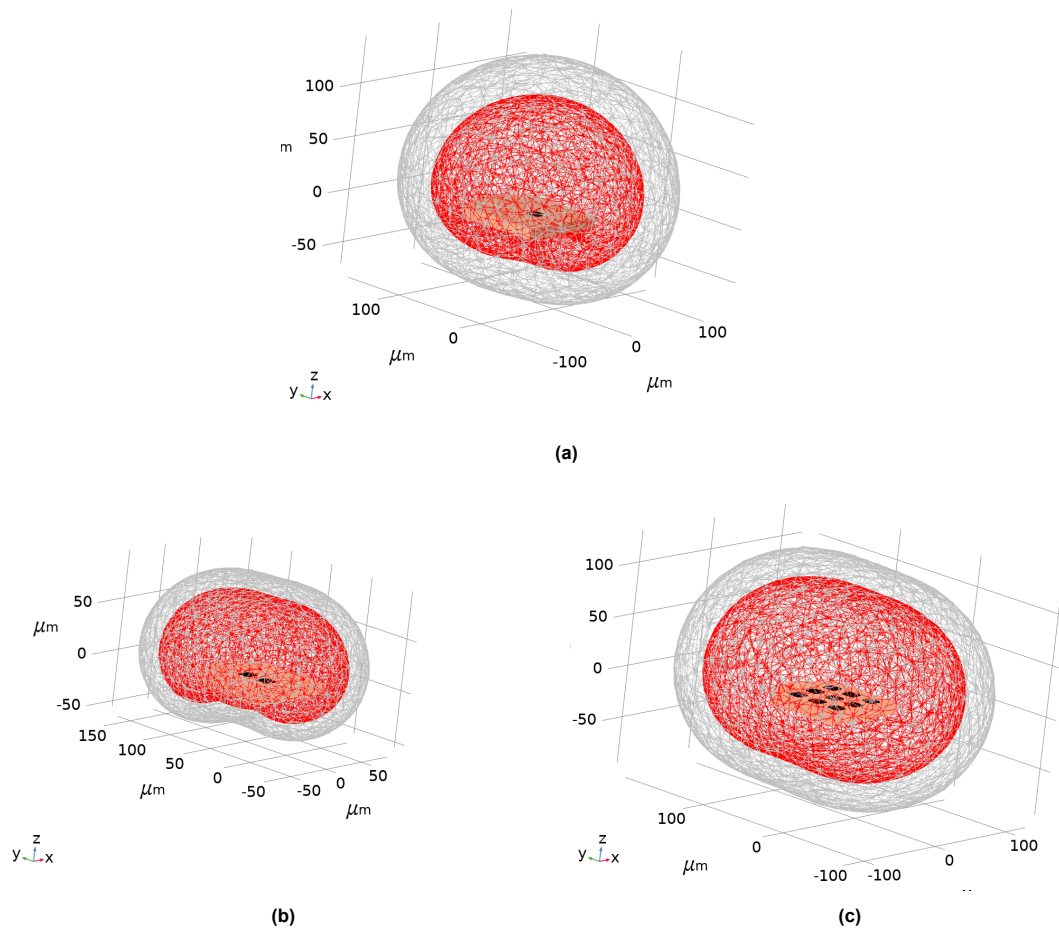


**Figure 4.13:** Surface density plots for a monopolar (a), bipolar (b) and a multipolar configuration (c). The sum of applied currents is equal to zero. The multipolar configuration uses model 3, as shown in Figure 4.12g.

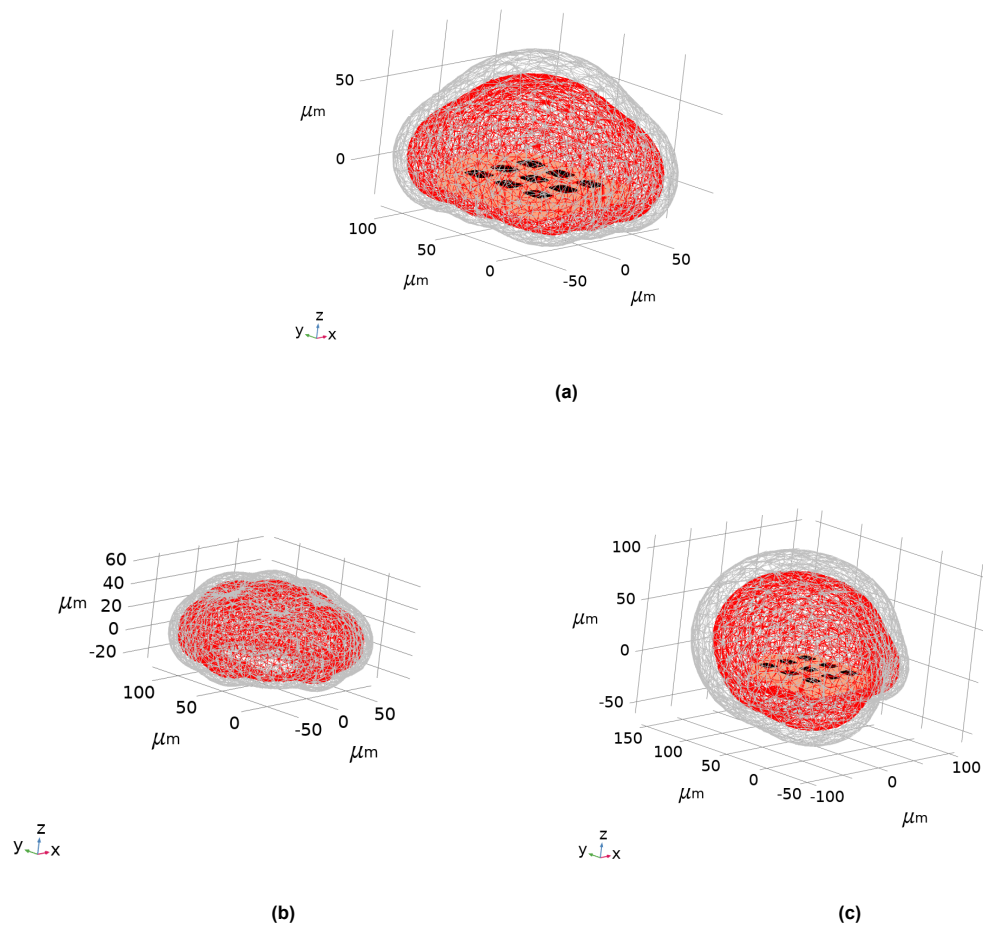


**Figure 4.14:** Surface density plots for varying current magnitudes of the multipolar electrode configuration model 2. It shows an application of  $+8 \mu A$  and  $-10 \mu A$  (a),  $+5/10 \mu A$  and  $-10 \mu A$  (b) and  $+5/10/20 \mu A$  and  $-15 \mu A$  (c). The sum of applied currents is equal to zero.

## 4.6. Neuronal activation using the activating function

Section 3.3 discussed how the activating function is a tool for approximating the spatial extent of neuronal stimulation. The success of neuronal activation can be estimated by examining the second spatial derivative of electric potential along a specified axis that is parallel to an axon. If the gradient of the generated electric potential is large enough, an action potential is initiated. Plotting the activating function reveals where stimulation induces a hyperpolarising or depolarising effect. This is illustrated in Figure 4.15. In the centre of a positive, stimulating contact, hyperpolarisation shall occur. As one moves away from the centre of the contact, the hyperpolarisation decreases and transitions towards slight depolarisation [52]. The panels at the left side show the generated potential and how this translates towards the activating function as a function along an axon. The other two panels show a visualisation of the Activating Function for fibres in different directions. These images show that the orientation of the fibre is relevant for selectively targeting certain regions.

Research has demonstrated that action potentials occur when the activating function surpasses threshold values of  $3 \text{ pA}/\mu\text{m}^2$  for myelinated fibres and  $60 \text{ pA}/\mu\text{m}^2$  for unmyelinated fibres [52]. By plotting the activating function with these thresholds, regions where neuronal stimulation is anticipated can be inspected. This is illustrated in Figure 4.16, which shows the corresponding areas of expected activation of a monopolar and bipolar electrode configuration. The plots visualise the regions where myelinated neurons orientated along the x-axis will be stimulated for an XY-plane at  $z = 15 \mu\text{m}$  above the surface of the electrode contacts.

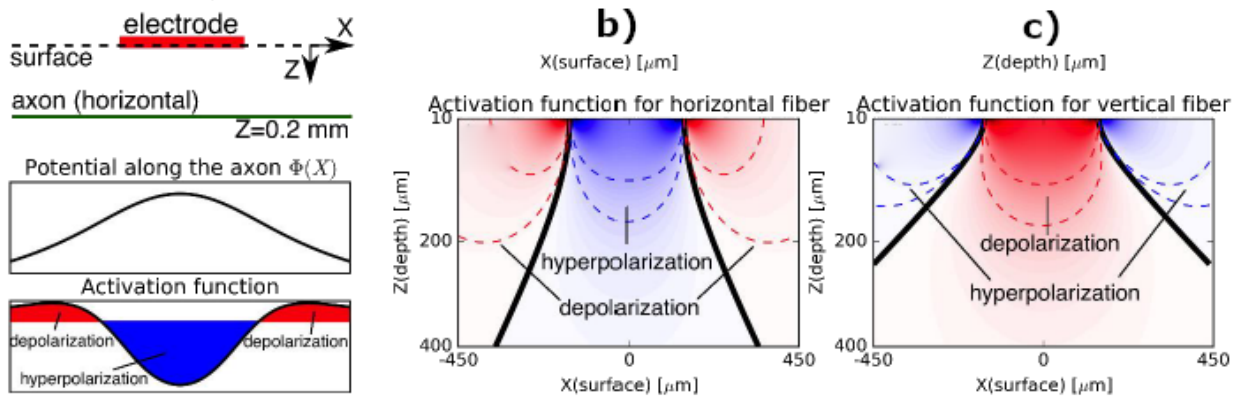


**Figure 4.15:** Schematic representation of the electrode (red) and horizontally oriented axon (green) on an XZ plane for  $Y=0$ . The next panels show the activating function for horizontally (b) and vertically (c) oriented fibres. Black solid curves separate areas of depolarisation (red) and hyperpolarisation (blue). This image is an adaptation from [52]

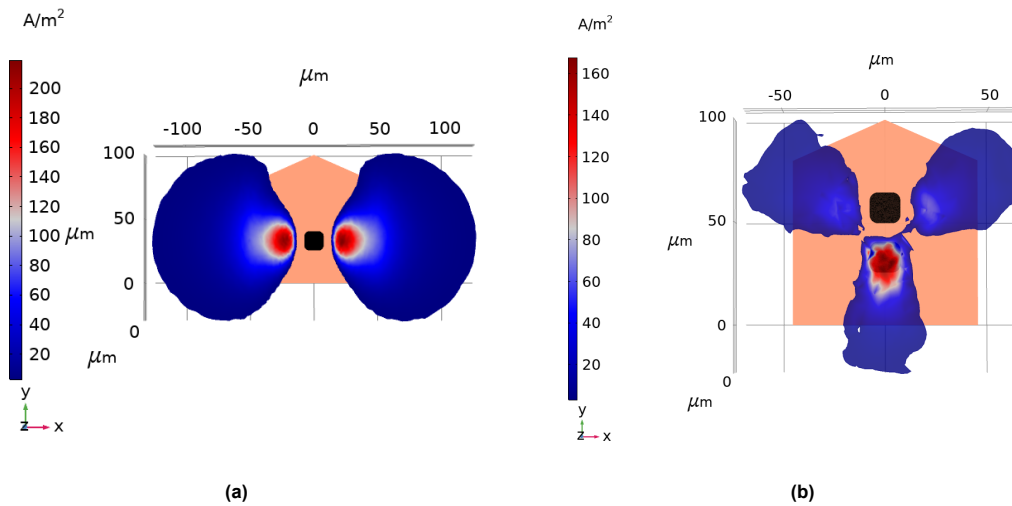


**Figure 4.16:** Plotted Activation Function in the x direction for a monopolar (a) and bipolar electrode contact configuration (b). The results have been filtered using the threshold for myelinated fibres ( $3 \text{ pA}/\mu\text{m}^2$ )

Similar results can be created for multipolar electrode contact configurations. This is shown in Figure 4.17. The multipolar configurations show that their generated stimulation regions have similar shapes to the mono and bipolar configurations but that the focus points of the stimulation have shifted. Changing the number of active contacts and polarity makes it possible to move the area of expected stimulation to create better-defined areas of stimulation. The effect of shifting becomes more pronounced when the applied current for each active contact is adjusted. While keeping the total sum of applied current equal to 0, it is possible to create variations of the same shape. This is shown in Figure 4.18.

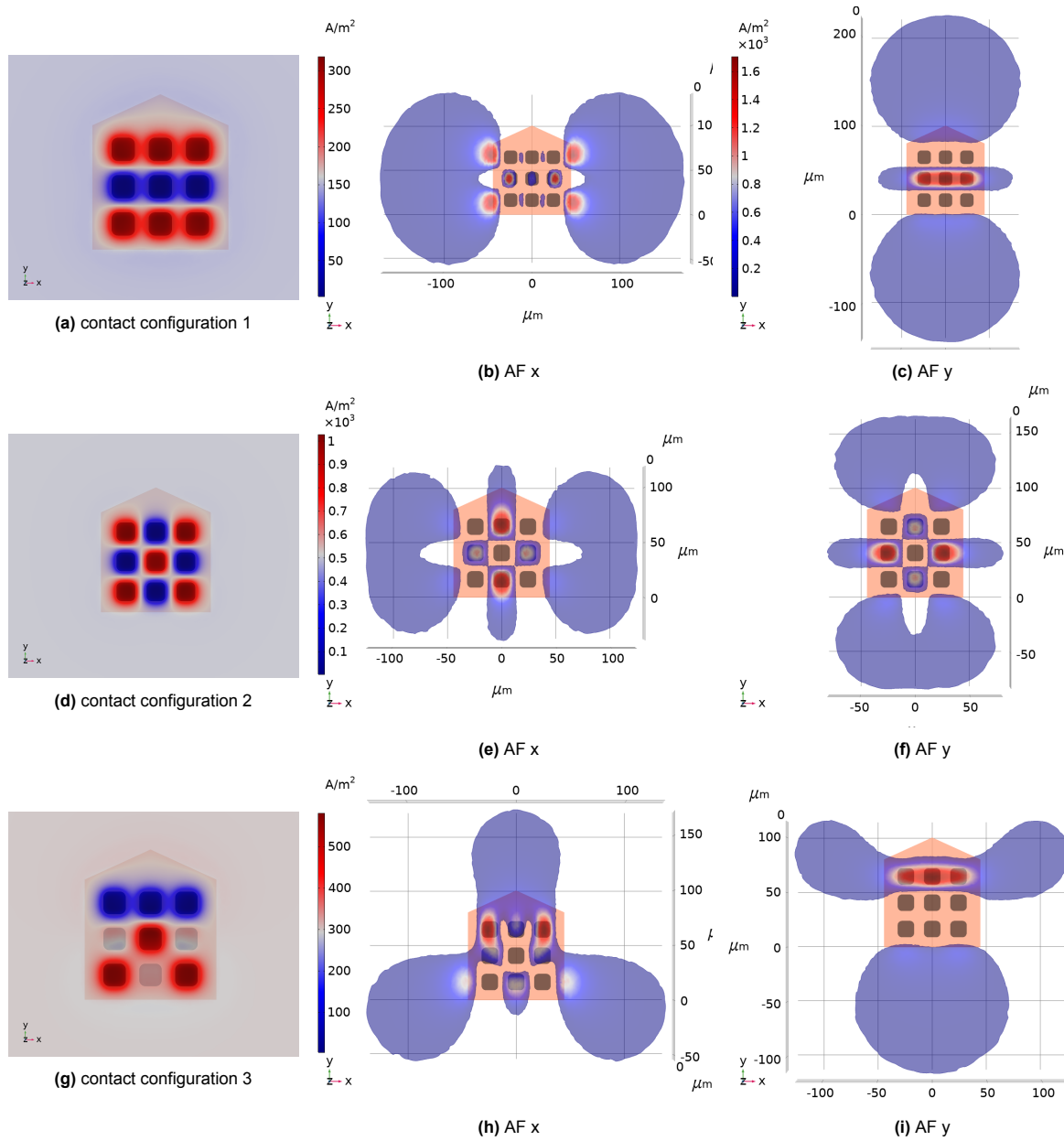


**Figure 4.17:** Demonstration of the differences between various electrode contact configurations and their corresponding Activating Function in x and y direction. The illustrated results are shown on an XY-plane  $15 \mu m$  above the contacts and are filtered to show activation areas for myelinated neurons in respectively x or y direction. ( $3 pA/\mu m^2$ )

The activating functions in the x and y direction of Figure 4.18 show examples of the application of current steering. It compares what happens to the solution when different electrode contact currents are applied to the same model. The model used for this demonstration is the contact configuration shown in Figure 4.17d. The minimal current applied to contact is  $5 \mu A$ , most use an applied current of  $10 \mu A$ , and the maximal applied current is  $20 \mu A$ . By strategically applying the currents while ensuring that the total applied sum of current equals zero (current conservation), the activation area can be shifted in different directions.

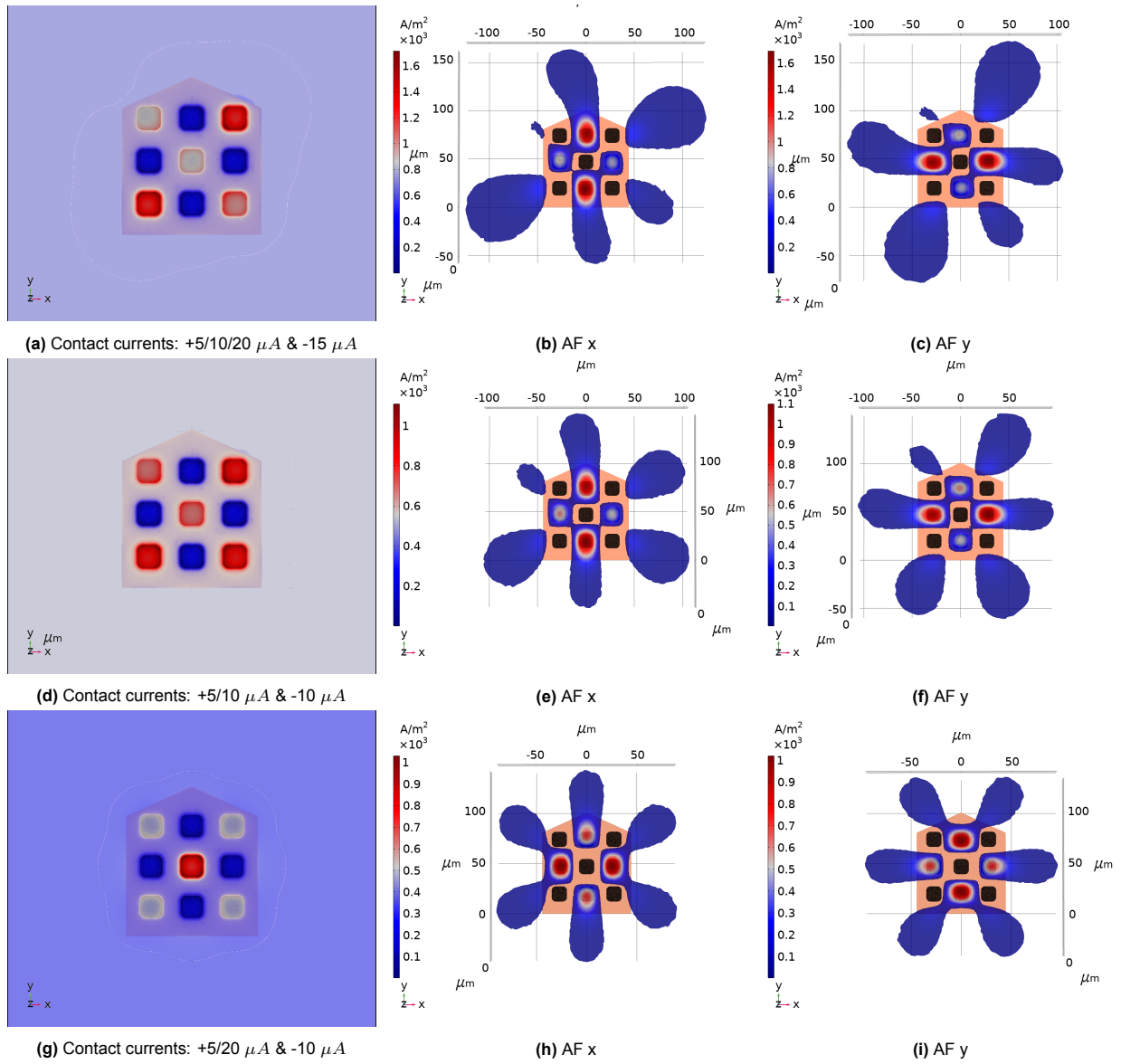


**Figure 4.18:** Examples of the effect of strategically changing the electrode contact currents on the Activating Function in x and y direction. The effect is shown for three variations of the applied currents using the same active contacts. The applied currents vary between 5 and 20  $\mu A$ . The results are shown on an XY plane 15  $\mu m$  above the contacts and are filtered for myelinated neurons (3  $pA/\mu m^2$ ).

## Discussion & Conclusion

This thesis addressed the question: *"How do we visualise the shape and intensity of electric fields in the cortex, considering electrode design parameters, to observe the expected activation region?"* From existing literature, it has been defined that there is a need to adequately confine the electric field generated by electrodes to focal regions due to its impact on the resolution of artificial vision in visual prostheses. Greater control over the shape of the electric fields and their impact on stimulation spread is wanted while considering the relation with electrode design parameters.

To simulate the effects of electrical stimulation on neuronal tissue, parameters that can influence the generated electric field and the regions of activated tissue have been defined. Implementing these parameters in a Finite Element Model (FEM) allows the computation of the generated electric field in 3D of a stimulating electrode to observe the volume of activated neuronal tissue. The volume of activated tissue can be estimated using simplified methods such as the activating function (AF) or the strength-distance relation. This thesis developed a framework that creates a Visualisation of Neuronal Activation (VoNA) that enables users to visualise the combined effects of alterations in electrode geometry and configurations to obtain the desired volumes of activated tissue.

### 5.1. Observations on the Influence of Model Parameters

The results presented in chapter 4 illustrate the strengths and capabilities of the designed tool. It shows how the model parameters can influence factors such as the generated electric field, the current density and electric potential, which are indicators of neuronal activation. The model allows the adjustment of the stimulation configuration (monopolar, bipolar, or multipolar), adjustment of electrode contact spacing (pitch), customisation of electrode size (length and width), and modulation of stimulation current. The key findings of observing the generated electric potential, electric field and current density will be discussed. The influence of model parameters on the expected volume of activation is discussed in the next section.

#### 5.1.1. The Influence on the Electric Potential, Field and Current Density

COMSOL allows us to solve the electrostatic fields using Poisson's equations for complex geometries considering electrical properties [49]. The dependent variable of the solution is the resulting electric potential. In line with expectations [28], the models show that changes in active electrode contact current, configuration, and location lead to varying electric potentials. The principle of superposition dictates that each electrode contact contributes to the generated electric potential, influencing the electric field's shape. Increasing the distance between contacts diminishes mutual influence, altering the respective applied voltage areas. This effect can also be seen when comparing the different electrode contact configurations. The monopolar electrode configuration yields a uniform electric potential; introducing more electrodes results in a confined electric potential matching the descriptions from the literature [30].

Analysing the generated electric field and the current density gives similar observations of the results because they are linearly related to the electric potential as  $\mathbf{E} = -\nabla V$  and  $J = \sigma E$  [105]. However, an important detail can be observed when comparing the electric field and current density across different electrode configurations. Directional variations are present in the electric field gradient and current density distribution. These variations in the distribution of the electric field change depending on the observation direction, becoming

more pronounced when using multiple active electrode contacts and varying their stimulation current, allowing targeted stimulation in specific regions. Similar observations are made in the analysis of the current density within the tissue. Comparing configurations highlights variations in shape and the total covered area. Altering applied contact currents while maintaining the same active contacts accentuates these variations. This effect aligns with expectation, as it describes the concept of current steering [32].

### 5.1.2. The influence on the current-distance relation and the activating function

The effective current spread from an electrode contact can be plotted using the current-distance relationship by determining the minimal required surface current density to indicate where neurons are likely to be stimulated. The minimal required surface current density covers a volume that mostly depends on the total applied stimulation current, making the results of the configurations pretty similar. Larger variations in the shape and covered volume of activated tissue are observed when comparing multipolar electrode configurations. By varying the applied contact currents while using the same active contacts, shifts of the activation area in different directions are observed. For example, an equal distribution among the positive and negative electrode contacts creates a peak in the centre above the electrode contacts. Creating a stronger stimulation on one side shifts the peak toward the more substantial current magnitudes.

Investigating the AF across the different configurations shows similar simulation results; the stimulation region shapes of the multipolar configuration are similar to mono- and bipolar configurations but with shifted focus points. Hyperpolarisation is observed near positive stimulating contacts and depolarization near negative contacts. Adding more active contacts reveals that the total covered area, as is the generated electric potential, is becoming more confined, creating well-defined regions. This effect intensifies with adjustments in applied current for each active contact, matching the application of current steering. These findings emphasise the utility of VoNA in comprehending and manipulating electric field characteristics based on electrode design parameters.

## 5.2. Model setup and limitations

The setup of the computational model is explained in chapter 3. The physics of the model considers the biophysical properties such as the electrical conductivity, the relative permittivity and possible dielectric properties. As a verification step, the total delivered current was calculated by integrating the current density over the outer boundaries of the model (assigned GND) to ensure current conservation [95]. The framework contains assumptions to allow the setup of this parameterised model. First, the model computes a solution for quasi-static conditions, neglecting transients of the applied current, only observing the generated electric potential directly after being applied. Second, the tissue is considered purely resistive and linear, while in reality, tissue's conductivity and dielectric constants generally vary with field frequency [100]. Next, the outer boundaries of the model have been grounded, and all potentials are initialized as 0 V. This assumption does not consider possible charges that could be present in the tissue. A current terminal boundary condition has modelled the electrode contacts, and any unused contacts are left floating to match findings from literature [49, 95, 106]. Using the Activating Function (AF) to approximate activation may not fully describe neuron responses for all distances and types of cells. This could result in overestimation or underestimation of neuron activation due to varying preferences of cell types regarding stimulation [52]. An alternative to the activating function could be the mirror estimate, which uses a simple estimate of membrane polarisation to form a better predictor of the steady-state solution [107].

## 5.3. Conclusion

The presented framework, VoNA, is a parameterised tool (and model) that can visualise the spatial extent of activated tissue regions for varying scenarios. Users can define the material properties and dimensions of the model to observe the volume of activated tissue for different electrode parameters. The selected parameters allow the adjustment of the stimulation configuration (monopolar, bipolar, or multipolar), adjustment of electrode contact spacing (pitch), customisation of electrode size (length and width), and modulation of stimulation current. It enables the user to tune the model settings towards their specific needs and explore the possibilities by visualising the results from different angles by defining subsets of the entire solution. For example, the results can be plotted in 3D to observe the resulting volume or observe space variations. When more details are required, the user can define a 2D plane or 1D points or cut lines to observe specific properties of that dataset.

## 5.4. Recommendations for future work

This section discusses recommendations for improving VoNA.

### 5.4.1. The implementation of the electrode tissue interface

Integrating the ETI into the model allows for a more accurate representation of the interactions between the electrode contacts and the surrounding neural tissue, enabling the observation of charge transfer mechanisms. The ETI represents the charge movement resulting from reversible and irreversible faradaic reactions and is represented by an equivalent electrical circuit of capacitance in parallel with a resistance. Due to the electrochemical double-layer formed by the polarisation of the electrode in the tissue, electrical charges can build up on the interface. The charge build-up should be prevented to avoid damaging the tissue. Therefore, including the ETI effects shall better represent the actual generated electric potential in tissue and allow the model to include safety considerations without increasing model complexity too much.

### 5.4.2. Adding glial scar encapsulation

Glial scars formation is a possible biological response to the insertion of electrodes. The presence of glial scar around the electrode changes the generated electric potential in tissue due to its influence on the ETI and electrode impedance and increases the distance between the electrode and targeted neurons, increasing the activation threshold. Modelling this effect can better represent the created electric field of electrodes implanted for a sustained period [78]. By adding encapsulation as an additional parameter in the tool, the impact of a glial scar on stimulation efficacy can be visualised by representing the glial scar as an adjustable volume of tissue with its properties.

### 5.4.3. Validation against other approaches

This thesis aimed to create a flexible and easy-to-use framework that does not require complicated steps before use. It is essential to compare the results from VoNA with the results from different approaches, such as a "whole FEM" or "hybrid" approach [108, 109], to verify the approximation of the neural activation. These models include complex cell membrane models that implement the neuron's passive (i.e., capacitance and leakage) and active (i.e., ion channels) characteristics. The transmembrane currents affect the potential distribution in the tissue [106]. Using these other approaches allows the determination of the model's accuracy against accurate but complex models without personally developing such a complex model.

### 5.4.4. The addition of a time-dependent simulation

By adding a time-dependent simulation, it is possible to include the stimulus properties, such as the timing, shape, and strength of the applied current. Adding these properties allows the user to investigate the generated electric field and the effect of the applied stimulus over time. It also allows the addition and observation of side effects such as frequency-dependent conductance, charge buildup, and heat development during the stimulation, which affects the neuronal response. By adding the time and frequency aspects, a more realistic estimation of the spatial extent of stimulation can be achieved.

### 5.4.5. Improving the application of the activating function

The activating function excels at approximating activation along a 1D fibre, but simulating neural activation in a 3D space would be even more beneficial. A possible approach is using the Hessian matrix, creating the second spatial partial derivatives of the electric potential in all directions [109].

### 5.4.6. Simulation of multiple electrode shanks

The current model consists of a single electrode shank with multiple stimulation contacts. Adding extra shanks to the model allows the simulation of more complex stimulation patterns. It also allows the user to research the changes in the electric field due to the presence of other shanks or stimulating contacts.

### 5.4.7. Adding more electrode contact parameters

It has been shown that the shape of the electrode contacts influences the generated electric potential. The user can currently only influence the electrode contacts' size, depth and pitch. By including different shapes or allowing the user to define the shape of the contact, it allows the comparison of the current distribution related to the electrode contact.



# References

- [1] W. Mayr, M. Krenn, and M. R. Dimitrijevic, "Neuroprosthetic Advances," *Innovative Neuromodulation*, pp. 209–234, Jan. 2017. DOI: [10.1016/B978-0-12-800454-8.00010-0](https://doi.org/10.1016/B978-0-12-800454-8.00010-0).
- [2] A. Kral, F. Aplin, and H. Maier, "History of neuroprostheses," in *Prostheses for the Brain*, Elsevier, Jan. 2021, pp. 19–31. DOI: [10.1016/B978-0-12-818892-7.00009-2](https://doi.org/10.1016/B978-0-12-818892-7.00009-2). [Online]. Available: <https://linkinghub.elsevier.com/retrieve/pii/B9780128188927000092>.
- [3] J. Fisher, S. Kim, S. Furman, and J. Matos, "Role of implantable pacemakers in control of recurrent ventricular tachycardia,"
- [4] X. Yao, H. Liu, J. Si, X. Ding, Y. Zhao, and Y. Zheng, "Research status and future development of cochlear reimplantation," *Frontiers in Neuroscience*, vol. 16, 2022, ISSN: 1662-453X. DOI: [10.3389/fnins.2022.824389](https://doi.org/10.3389/fnins.2022.824389). [Online]. Available: <https://www.frontiersin.org/articles/10.3389/fnins.2022.824389>.
- [5] S. N. Serva, J. Bernstein, J. A. Thompson, D. S. Kern, and S. G. Ojemann, "An update on advanced therapies for parkinson's disease: From gene therapy to neuromodulation," *Frontiers in Surgery*, vol. 9, 2022, ISSN: 2296-875X. DOI: [10.3389/fsurg.2022.863921](https://doi.org/10.3389/fsurg.2022.863921). [Online]. Available: <https://www.frontiersin.org/articles/10.3389/fsurg.2022.863921>.
- [6] R. A. Normann, D. J. Warren, J. Ammermuller, E. Fernandez, and S. Guillory, "High-resolution spatio-temporal mapping of visual pathways using multi-electrode arrays," *Vision Research*, vol. 41, no. 10, pp. 1261–1275, 2001, ISSN: 0042-6989. DOI: [https://doi.org/10.1016/S0042-6989\(00\)00273-X](https://doi.org/10.1016/S0042-6989(00)00273-X). [Online]. Available: <https://www.sciencedirect.com/science/article/pii/S004269890000273X>.
- [7] J. Sommerhalder, A. P. Fornos, J. Sommerhalder, and A. P. Fornos, "Prospects and Limitations of Spatial Resolution," *Artificial Vision*, pp. 29–45, 2017. DOI: [10.1007/978-3-319-41876-6{\\\\_}4](https://doi.org/10.1007/978-3-319-41876-6{\\_}4). [Online]. Available: [https://link-springer-com.tudelft.idm.oclc.org/chapter/10.1007/978-3-319-41876-6\\_4](https://link-springer-com.tudelft.idm.oclc.org/chapter/10.1007/978-3-319-41876-6_4).
- [8] H. Ye, J. Hendee, J. Ruan, A. Zhirova, J. Ye, and M. Dima, "Neuron matters: neuromodulation with electromagnetic stimulation must consider neurons as dynamic identities," *Journal of NeuroEngineering and Rehabilitation* 2022 19:1, vol. 19, no. 1, pp. 1–14, Nov. 2022, ISSN: 1743-0003. DOI: [10.1186/S12984-022-01094-4](https://doi.org/10.1186/S12984-022-01094-4). [Online]. Available: <https://jneuroengrehab.biomedcentral.com/articles/10.1186/s12984-022-01094-4>.
- [9] A. Kral, F. Aplin, and H. Maier, "Visual neuroprostheses," *Prostheses for the Brain*, pp. 251–289, Jan. 2021. DOI: [10.1016/B978-0-12-818892-7.00011-0](https://doi.org/10.1016/B978-0-12-818892-7.00011-0).
- [10] e. a. Purves D., *Neuroscience. 6th Edition*. Oxford university Press Inc, 2018, ISBN: 9781538619377.
- [11] F. N, T. H, T. M, H. N, A. K, and Y. H. N. H, "Lateral geniculate nucleus: Anatomic and functional identification by use of mr imaging," *American journal of neuroradiology*, vol. 9, pp. 1719–1726, 2001.
- [12] C. Stangor and J. Walinga, "Introduction to psychology," 2010. [Online]. Available: [Available:%20https://opentextbc.ca/introductiontopsychology/](https://opentextbc.ca/introductiontopsychology/).
- [13] "Opthamology training, "visual cortex",," (accessed: july. 20, 2023) [Online]. [Online]. Available: [//www.opthamologytraining.com/core-principles/ocular-anatomy/visual-pathway/visual-cortex](http://www.opthamologytraining.com/core-principles/ocular-anatomy/visual-pathway/visual-cortex).
- [14] E. Fernandez and R. Normann, "Introduction to visual prostheses," 2016. [Online]. Available: <http://www.ncbi.nlm.nih.gov/pubmed/27809426>.
- [15] B. A. Wandell and J. Winawer, "Imaging retinotopic maps in the human brain," *Vision Research*, vol. 51, no. 7, pp. 718–737, Apr. 2011, ISSN: 0042-6989. DOI: [10.1016/J.VISRES.2010.08.004](https://doi.org/10.1016/J.VISRES.2010.08.004).
- [16] M. Ibbotson and Y. J. Jung, "Origins of Functional Organization in the Visual Cortex," *Frontiers in Systems Neuroscience*, vol. 14, p. 503 882, Mar. 2020, ISSN: 16625137. DOI: [10.3389/FNSYS.2020.00010/BIBTEX](https://doi.org/10.3389/FNSYS.2020.00010/BIBTEX).

- [17] E. J. Tehovnik, W. M. Slocum, S. M. Smirnakis, and A. S. Tolia, "Microstimulation of visual cortex to restore vision," *Progress in brain research*, vol. 175, pp. 347–375, 2009.
- [18] S. e. a. Ramaswamy, *Microcircuitry of the neocortex*. Oxford university Press Inc, 2018, ISBN: 978-0-19-063611-1.
- [19] A. Kral, F. Aplin, and H. Maier, *Prostheses for the Brain*. Academic Press, 2021, pp. 353–386, ISBN: 978-0-12-818892-7. DOI: <https://doi.org/10.1016/B978-0-12-818892-7.00017-1>. [Online]. Available: <https://www.sciencedirect.com/science/article/pii/B9780128188927000171>.
- [20] M. Schmolesky, "The primary visual cortex," pp. 1039–1070, 2005. [Online]. Available: [https://www.ncbi.nlm.nih.gov/books/NBK11524/pdf/Bookshelf\\_%20NBK11524.pdf](https://www.ncbi.nlm.nih.gov/books/NBK11524/pdf/Bookshelf_%20NBK11524.pdf).
- [21] "Foundations of neuroscience." (2023), [Online]. Available: <https://openbooks.lib.msu.edu/neuroscience/chapter/the-neuron/> (visited on 11/24/2023).
- [22] P. L. Nunez and R. Srinivasan, "Chapter 4 - Electric Fields and Currents in Biological Tissue," *Electric fields of the Brain: The neurophysics of EEG*, 2006. DOI: [10.1093/acprof:oso/9780195050387.001.0001](https://doi.org/10.1093/acprof:oso/9780195050387.001.0001).
- [23] A. Kral, F. Aplin, and H. Maier, "Neuronal excitation," *Prostheses for the Brain*, pp. 55–75, Jan. 2021. DOI: [10.1016/B978-0-12-818892-7.00003-1](https://doi.org/10.1016/B978-0-12-818892-7.00003-1).
- [24] J. Moini, N. G. Avgeropoulos, and M. Samsam, "Chapter 2 - cytology of the nervous system," in *Epidemiology of Brain and Spinal Tumors*, J. Moini, N. G. Avgeropoulos, and M. Samsam, Eds., Academic Press, 2021, pp. 41–63, ISBN: 978-0-12-821736-8. DOI: <https://doi.org/10.1016/B978-0-12-821736-8.00012-1>. [Online]. Available: <https://www.sciencedirect.com/science/article/pii/B9780128217368000121>.
- [25] D. Chambers, C. Huang, and G. Matthews, "Nerve Action Potential and Propagation," *Basic Physiology for Anaesthetists*, pp. 225–230, Jul. 2019. DOI: [10.1017/9781108565011.055](https://doi.org/10.1017/9781108565011.055). [Online]. Available: <https://www-cambridge-org.tudelft.idm.oclc.org/core/books/basic-physiology-for-anaesthetists/nerve-action-potential-and-propagation/31B6C11A49B20CC69D3EB1E5CCCFB208>.
- [26] E. J. Tehovnik, A. S. Tolia, F. Sultan, W. M. Slocum, and N. K. Logothetis, *Direct and indirect activation of cortical neurons by electrical microstimulation*, 2006. DOI: [10.1152/jn.00126.2006](https://doi.org/10.1152/jn.00126.2006).
- [27] A. Kral, F. Aplin, and H. Maier, "Artificial electrical stimulation: Principles, efficacy, and safety," *Prostheses for the Brain*, pp. 95–113, Jan. 2021. DOI: [10.1016/B978-0-12-818892-7.00008-0](https://doi.org/10.1016/B978-0-12-818892-7.00008-0).
- [28] Z. Gilbert *et al.*, "A review of neurophysiological effects and efficiency of waveform parameters in deep brain stimulation," *Clinical Neurophysiology*, vol. 152, pp. 93–111, Aug. 2023, ISSN: 1388-2457. DOI: [10.1016/J.CLINPH.2023.04.007](https://doi.org/10.1016/J.CLINPH.2023.04.007).
- [29] J. Simpson and M. Ghovanloo, "An experimental study of voltage, current, and charge controlled stimulation front-end circuitry," *Proceedings - IEEE International Symposium on Circuits and Systems*, pp. 325–328, 2007, ISSN: 02714310. DOI: [10.1109/ISCAS.2007.378401](https://doi.org/10.1109/ISCAS.2007.378401).
- [30] A. Kral, F. Aplin, and H. Maier, "Stimulation rules," *Prostheses for the Brain*, pp. 115–134, Jan. 2021. DOI: [10.1016/B978-0-12-818892-7.00002-X](https://doi.org/10.1016/B978-0-12-818892-7.00002-X).
- [31] S. J. Meikle, M. Ann Hagan, N. S. Chiang Price, and Y. Tat Wong, "Filling in the Visual Gaps: Shifting Cortical Activity using Current Steering," in *2021 43rd Annual International Conference of the IEEE Engineering in Medicine & Biology Society (EMBC)*, IEEE, Nov. 2021, pp. 5733–5736, ISBN: 978-1-7281-1179-7. DOI: [10.1109/EMBC46164.2021.9629693](https://doi.org/10.1109/EMBC46164.2021.9629693). [Online]. Available: <https://ieeexplore.ieee.org/document/9629693/>.
- [32] Z. C. Chen, B.-Y. Wang, and D. Palanker, "Real-Time Optimization of the Current Steering for Visual Prosthesis," *International IEEE/EMBS Conference on Neural Engineering (NER)*, 2020. [Online]. Available: <http://arxiv.org/abs/2012.13467>.
- [33] M. S. Humayun, R. A. Brant Fernandes, and J. D. Weiland, "Artificial Vision," *Retina Fifth Edition*, pp. 2078–2093, Jan. 2013. DOI: [10.1016/B978-1-4557-0737-9.00126-0](https://doi.org/10.1016/B978-1-4557-0737-9.00126-0).
- [34] T. Sharf, T. Kalakuntla, D. J Lee, and K. K. Gokoffski, "Electrical devices for visual restoration," *Survey of Ophthalmology*, vol. 67, no. 3, pp. 793–800, May 2022, ISSN: 0039-6257. DOI: [10.1016/J.SURVOPHTHAL.2021.08.008](https://doi.org/10.1016/J.SURVOPHTHAL.2021.08.008).

- [35] R. A. Normann and E. Fernandez, "Clinical applications of penetrating neural interfaces and Utah Electrode Array technologies," *Journal of Neural Engineering*, vol. 13, no. 6, p. 061003, Oct. 2016, ISSN: 1741-2552. DOI: [10.1088/1741-2552/13/6/061003](https://doi.org/10.1088/1741-2552/13/6/061003). [Online]. Available: <https://iopscience-iop-org.tudelft.idm.oclc.org/article/10.1088/1741-2552/13/6/061003%20https://iopscience-iop-org.tudelft.idm.oclc.org/article/10.1088/1741-2552/13/6/061003/meta>.
- [36] T. S. Davis and R. A. Normann, "Visual percepts evoked with an intracortical 96-channel microelectrode array inserted in human occipital cortex," *Journal of Clinical Investigation*, vol. 131, no. 23, 2021. DOI: [10.1172/JCI151331](https://doi.org/10.1172/JCI151331).
- [37] P. M. Lewis, H. M. Ackland, A. J. Lowery, and J. V. Rosenfeld, "Restoration of vision in blind individuals using bionic devices: A review with a focus on cortical visual prostheses," *Brain Research*, vol. 1595, pp. 51–73, Jan. 2015, ISSN: 0006-8993. DOI: [10.1016/J.BRAINRES.2014.11.020](https://doi.org/10.1016/J.BRAINRES.2014.11.020).
- [38] L. Pio-Lopez, R. Poulkouras, and D. Depannemaecker, "Visual cortical prosthesis: an electrical perspective," *Journal of Medical Engineering & Technology*, vol. 45, no. 5, pp. 394–407, 2021, ISSN: 1464522X. DOI: [10.1080/03091902.2021.1907468](https://doi.org/10.1080/03091902.2021.1907468). [Online]. Available: <https://www-tandfonline-com.tudelft.idm.oclc.org/doi/abs/10.1080/03091902.2021.1907468>.
- [39] A. Najarpour Foroushani, C. C. Pack, and M. Sawan, "Cortical visual prostheses: from microstimulation to functional percept," *Journal of Neural Engineering*, vol. 15, no. 2, p. 021005, Feb. 2018, ISSN: 1741-2552. DOI: [10.1088/1741-2552/AAA904](https://doi.org/10.1088/1741-2552/AAA904). [Online]. Available: <https://iopscience-iop-org.tudelft.idm.oclc.org/article/10.1088/1741-2552/aaa904%20https://iopscience-iop-org.tudelft.idm.oclc.org/article/10.1088/1741-2552/aaa904/meta>.
- [40] V. P. Gabel, "Artificial Vision A Clinical Guide," Tech. Rep.
- [41] K. Torab, T. S. Davis, D. J. Warren, P. A. House, R. A. Normann, and B. Greger, "Multiple factors may influence the performance of a visual prosthesis based on intracortical microstimulation: nonhuman primate behavioural experimentation," *Journal of Neural Engineering*, vol. 8, no. 3, p. 035001, May 2011, ISSN: 1741-2552. DOI: [10.1088/1741-2552/8/3/035001](https://doi.org/10.1088/1741-2552/8/3/035001). [Online]. Available: <https://iopscience-iop-org.tudelft.idm.oclc.org/article/10.1088/1741-2552/8/3/035001%20https://iopscience-iop-org.tudelft.idm.oclc.org/article/10.1088/1741-2552/8/3/035001/meta>.
- [42] M. E. Urdaneta, A. S. Koivuniemi, and K. J. Otto, "Central nervous system microstimulation: Towards selective micro-neuromodulation," *Current Opinion in Biomedical Engineering*, vol. 4, pp. 65–77, Dec. 2017, ISSN: 2468-4511. DOI: [10.1016/J.COBME.2017.09.012](https://doi.org/10.1016/J.COBME.2017.09.012).
- [43] F. Rattay, S. M. Danner, U. S. Hofstoetter, and K. Minassian, "Finite Element Modeling for Extracellular Stimulation," in *Encyclopedia of Computational Neuroscience*, New York, NY: Springer New York, 2013, pp. 1–12, ISBN: 9781461473206. DOI: [10.1007/978-1-4614-7320-6\\_593-4](https://doi.org/10.1007/978-1-4614-7320-6_593-4). [Online]. Available: [http://link.springer.com/10.1007/978-1-4614-7320-6\\_593-4](http://link.springer.com/10.1007/978-1-4614-7320-6_593-4).
- [44] M. Raghavan, D. Fee, and P. E. Barkhaus, "Generation and propagation of the action potential," *Handbook of Clinical Neurology*, vol. 160, pp. 3–22, Jan. 2019, ISSN: 0072-9752. DOI: [10.1016/B978-0-444-64032-1.00001-1](https://doi.org/10.1016/B978-0-444-64032-1.00001-1).
- [45] Wikipedia. "Cable theory." (2017), [Online]. Available: [https://en.wikipedia.org/wiki/Cable\\_theory](https://en.wikipedia.org/wiki/Cable_theory) (visited on 12/24/2023).
- [46] A. Kral, F. Aplin, and H. Maier, "Electrode-tissue interface," *Prostheses for the Brain*, pp. 77–93, Jan. 2021. DOI: [10.1016/B978-0-12-818892-7.00004-3](https://doi.org/10.1016/B978-0-12-818892-7.00004-3).
- [47] C. R. Johnson, "Computational and numerical methods for bioelectric field problems," *Critical reviews in biomedical engineering*, vol. 25, no. 1, pp. 1–81, 1997, ISSN: 0278-940X. DOI: [10.1615/CRITREVB IOMEDENG.V25.I1.10](https://doi.org/10.1615/CRITREVB IOMEDENG.V25.I1.10). [Online]. Available: <https://pubmed.ncbi.nlm.nih.gov/9222078/>.
- [48] S. Joucla, A. Glière, and B. Yvert, "Current approaches to model extracellular electrical neural microstimulation," *Frontiers in Computational Neuroscience*, vol. 8, no. FEB, p. 49762, Feb. 2014, ISSN: 16625188. DOI: [10.3389/FNCOM.2014.00013/ABSTRACT](https://doi.org/10.3389/FNCOM.2014.00013/ABSTRACT).
- [49] A. Fellner, A. Heshmat, P. Werginz, and F. Rattay, "A finite element method framework to model extracellular neural stimulation," *Journal of Neural Engineering*, vol. 19, no. 2, Apr. 2022, ISSN: 17412552. DOI: [10.1088/1741-2552/ac6060](https://doi.org/10.1088/1741-2552/ac6060).
- [50] F. Rattay, "Analysis of Models for Extracellular Fiber Stimulation," *IEEE Transactions on Biomedical Engineering*, vol. 36, no. 7, pp. 676–682, 1989, ISSN: 15582531. DOI: [10.1109/10.32099](https://doi.org/10.1109/10.32099).

- [51] L. Butenko, "Deep brain stimulation: Activated axons vs. activation functions," *Frontiers in Neuroscience*, vol. 16, p. 625 119, 2022.
- [52] M. Komarov, P. Malerba, R. Golden, P. Nunez, E. Halgren, and M. Bazhenov, "Selective recruitment of cortical neurons by electrical stimulation," *PLoS Computational Biology*, vol. 15, no. 8, 2019, ISSN: 15537358. DOI: [10.1371/journal.pcbi.1007277](https://doi.org/10.1371/journal.pcbi.1007277).
- [53] E. Borda and D. Ghezzi, "Progress in Biomedical Engineering," 2022. DOI: [10.1088/2516-1091/ac812c](https://doi.org/10.1088/2516-1091/ac812c). [Online]. Available: <https://doi.org/10.1088/2516-1091/ac812c>.
- [54] X. Liu *et al.*, "A narrative review of cortical visual prosthesis systems: the latest progress and significance of nanotechnology for the future," *Annals of Translational Medicine*, vol. 10, no. 12, pp. 716–716, Jun. 2022, ISSN: 23055839. DOI: [10.21037/ATM-22-2858](https://doi.org/10.21037/ATM-22-2858). [Online]. Available: [/pmc/articles/PMC9279795/](https://pubmed.ncbi.nlm.nih.gov/pmc/articles/PMC9279795/) [https://www.ncbi.nlm.nih.gov/pmc/articles/PMC9279795/](https://www.ncbi.nlm.nih.gov/pmc/articles/PMC9279795/?report=abstract%20https://www.ncbi.nlm.nih.gov/pmc/articles/PMC9279795/).
- [55] P. R. Troyk and P. R. Troyk, "The Intracortical Visual Prosthesis Project," *Artificial Vision*, pp. 203–214, 2017. DOI: [10.1007/978-3-319-41876-6\\_16](https://doi.org/10.1007/978-3-319-41876-6_16). [Online]. Available: [https://link-springer-com.tudelft.idm.oclc.org/chapter/10.1007/978-3-319-41876-6\\_16](https://link.springer.com/tudelft.idm.oclc.org/chapter/10.1007/978-3-319-41876-6_16).
- [56] A. J. Lowery *et al.*, "Monash Vision Group's Gennaris Cortical Implant for Vision Restoration," *Artificial Vision*, pp. 215–225, 2017. DOI: [10.1007/978-3-319-41876-6\\_17](https://doi.org/10.1007/978-3-319-41876-6_17). [Online]. Available: [https://link.springer.com/chapter/10.1007/978-3-319-41876-6\\_17](https://link.springer.com/chapter/10.1007/978-3-319-41876-6_17).
- [57] J. V. Rosenfeld *et al.*, "Tissue response to a chronically implantable wireless intracortical visual prosthesis (Gennaris array)," *Journal of Neural Engineering*, vol. 17, no. 4, p. 046 001, Jul. 2020, ISSN: 1741-2552. DOI: [10.1088/1741-2552/AB9E1C](https://doi.org/10.1088/1741-2552/AB9E1C). [Online]. Available: <https://iopscience.iop.org/article/10.1088/1741-2552/ab9e1c%20https://iopscience.iop.org/article/10.1088/1741-2552/ab9e1c/meta>.
- [58] E. Fernández and R. A. Normann, "CORTIVIS Approach for an Intracortical Visual Prostheses," *Artificial Vision*, pp. 191–201, 2017. DOI: [10.1007/978-3-319-41876-6\\_15](https://doi.org/10.1007/978-3-319-41876-6_15).
- [59] S. Niketeghad and N. Pouratian, "Brain Machine Interfaces for Vision Restoration: The Current State of Cortical Visual Prosthetics," *Neurotherapeutics*, vol. 16, no. 1, pp. 134–143, Jan. 2019, ISSN: 18787479. DOI: [10.1007/S13311-018-0660-1/FIGURES/4](https://doi.org/10.1007/S13311-018-0660-1/FIGURES/4). [Online]. Available: <https://link-springer-com.tudelft.idm.oclc.org/article/10.1007/s13311-018-0660-1>.
- [60] Y. T. Wong *et al.*, "CMOS stimulating chips capable of wirelessly driving 473 electrodes for a cortical vision prosthesis," *Journal of neural engineering*, vol. 16, no. 2, Feb. 2019, ISSN: 1741-2552. DOI: [10.1088/1741-2552/AB021B](https://doi.org/10.1088/1741-2552/AB021B). [Online]. Available: <https://pubmed.ncbi.nlm.nih.gov/30690434/>.
- [61] L. Y. Cabrera and D. J. Weber, "Rethinking the ethical priorities for brain–computer interfaces," *Nature Electronics*, Feb. 2023, ISSN: 2520-1131. DOI: [10.1038/s41928-023-00928-w](https://doi.org/10.1038/s41928-023-00928-w). [Online]. Available: <https://www.nature.com/articles/s41928-023-00928-w>.
- [62] R. Yuste *et al.*, "Four ethical priorities for neurotechnologies and AI," *Nature* 2017 551:7679, vol. 551, no. 7679, pp. 159–163, Nov. 2017, ISSN: 1476-4687. DOI: [10.1038/551159A](https://doi.org/10.1038/551159A). [Online]. Available: <https://www-nature-com.tudelft.idm.oclc.org/articles/551159a>.
- [63] L. De Levy Oliveira, N. Suematsu, and T. Yagi, "Spatiotemporal Analysis of Simultaneous Repetitive Electrical Stimulation with Voltage Sensitive Dye," *2018 IEEE Biomedical Circuits and Systems Conference, BioCAS 2018 - Proceedings*, no. C, pp. 9–12, 2018. DOI: [10.1109/BIOCAS.2018.8584719](https://doi.org/10.1109/BIOCAS.2018.8584719).
- [64] H. Subhi, K. Latham, J. Myint, and M. D. Crossland, "Functional visual fields: relationship of visual field areas to self-reported function," *Ophthalmic & physiological optics : the journal of the British College of Ophthalmic Opticians (Optometrists)*, vol. 37, no. 4, pp. 399–408, Jul. 2017, ISSN: 1475-1313. DOI: [10.1111/OP0.12362](https://doi.org/10.1111/OP0.12362). [Online]. Available: <https://pubmed.ncbi.nlm.nih.gov/28281282/>.
- [65] K. Cha, K. Horsch, and R. A. Normann, "Simulation of a phosphene-based visual field: visual acuity in a pixelized vision system," *Annals of biomedical engineering*, vol. 20, no. 4, pp. 439–449, Jul. 1992, ISSN: 0090-6964. DOI: [10.1007/BF02368135](https://doi.org/10.1007/BF02368135). [Online]. Available: <https://pubmed.ncbi.nlm.nih.gov/1510295/>.



- [66] M. H. Histed, V. Bonin, and R. C. Reid, "Direct activation of sparse, distributed populations of cortical neurons by electrical microstimulation," *Neuron*, vol. 63, no. 4, pp. 508–522, Aug. 2009, ISSN: 1097-4199. DOI: [10.1016/J.NEURON.2009.07.016](https://doi.org/10.1016/J.NEURON.2009.07.016). [Online]. Available: <https://pubmed-ncbi-nlm-nih-gov.tudelft.idm.oclc.org/19709632/>.
- [67] X. Chen, F. Wang, E. Fernandez, and P. R. Roelfsema, "Shape perception via a high-channel-count neuroprosthesis in monkey visual cortex," *Science (New York, N.Y.)*, vol. 370, no. 6521, Dec. 2020, ISSN: 1095-9203. DOI: [10.1126/SCIENCE.ABD7435](https://doi.org/10.1126/SCIENCE.ABD7435). [Online]. Available: <https://pubmed.ncbi.nlm.nih.gov/33273097/>.
- [68] M. S. Beauchamp *et al.*, "Dynamic Stimulation of Visual Cortex Produces Form Vision in Sighted and Blind Humans," *Cell*, vol. 181, no. 4, pp. 774–783, May 2020, ISSN: 10974172. DOI: [10.1016/j.cell.2020.04.033](https://doi.org/10.1016/j.cell.2020.04.033). [Online]. Available: <https://doi.org/10.1016/j.cell.2020.04.033%20https://linkinghub.elsevier.com/retrieve/pii/S0092867420304967>.
- [69] V. Vergnien, M. J. Macé, and C. Jouffrais, "Simplification of Visual Rendering in Simulated Prosthetic Vision Facilitates Navigation," *Artificial organs*, vol. 41, no. 9, pp. 852–861, Sep. 2017, ISSN: 1525-1594. DOI: [10.1111/AOR.12868](https://doi.org/10.1111/AOR.12868). [Online]. Available: <https://pubmed.ncbi.nlm.nih.gov/28321887/>.
- [70] F. I. Kiral-Kornek, C. O. Savage, E. O'Sullivan-Greene, A. N. Burkitt, and D. B. Grayden, "Embracing the irregular: a patient-specific image processing strategy for visual prostheses," *Annual International Conference of the IEEE Engineering in Medicine and Biology Society. IEEE Engineering in Medicine and Biology Society. Annual International Conference*, vol. 2013, pp. 3563–3566, 2013, ISSN: 2694-0604. DOI: [10.1109/EMBC.2013.6610312](https://doi.org/10.1109/EMBC.2013.6610312). [Online]. Available: <https://pubmed.ncbi.nlm.nih.gov/24110499/>.
- [71] L. B. Merabet, J. F. Rizzo, A. Pascual-Leone, and E. Fernandez, "'Who is the ideal candidate?': decisions and issues relating to visual neuroprosthesis development, patient testing and neuroplasticity," *Journal of neural engineering*, vol. 4, no. 1, Mar. 2007, ISSN: 1741-2560. DOI: [10.1088/1741-2560/4/1/S15](https://doi.org/10.1088/1741-2560/4/1/S15). [Online]. Available: <https://pubmed.ncbi.nlm.nih.gov/17325411/>.
- [72] A. Lozano *et al.*, "Neurolight Alpha: Interfacing Computational Neural Models for Stimulus Modulation in Cortical Visual Neuroprostheses," *Lecture Notes in Computer Science (including subseries Lecture Notes in Artificial Intelligence and Lecture Notes in Bioinformatics)*, vol. 11486 LNCS, pp. 108–119, 2019, ISSN: 16113349. DOI: [10.1007/978-3-030-19591-5\\_12](https://doi.org/10.1007/978-3-030-19591-5_12). [Online]. Available: [https://link.springer.com/chapter/10.1007/978-3-030-19591-5\\_12](https://link.springer.com/chapter/10.1007/978-3-030-19591-5_12).
- [73] G. L. Barbruni, P. M. Ros, D. Demarchi, S. Carrara, and D. Ghezzi, "Miniaturised Wireless Power Transfer Systems for Neurostimulation: A Review," *IEEE transactions on biomedical circuits and systems*, vol. 14, no. 6, pp. 1160–1178, Dec. 2020, ISSN: 1940-9990. DOI: [10.1109/TBCAS.2020.3038599](https://doi.org/10.1109/TBCAS.2020.3038599). [Online]. Available: <https://pubmed.ncbi.nlm.nih.gov/33201828/>.
- [74] L. N. Ayton *et al.*, "An update on retinal prostheses," *Clinical neurophysiology : official journal of the International Federation of Clinical Neurophysiology*, vol. 131, no. 6, pp. 1383–1398, Jun. 2020, ISSN: 1872-8952. DOI: [10.1016/J.CLINPH.2019.11.029](https://doi.org/10.1016/J.CLINPH.2019.11.029). [Online]. Available: <https://pubmed.ncbi.nlm.nih.gov/31866339/>.
- [75] W. H. Bosking, M. S. Beauchamp, and D. Yashor, "Electrical Stimulation of Visual Cortex: Relevance for the Development of Visual Cortical Prosthetics," *Annual review of vision science*, vol. 3, p. 141, Sep. 2017, ISSN: 23744650. DOI: [10.1146/ANNUREV-VISION-111815-114525](https://doi.org/10.1146/ANNUREV-VISION-111815-114525). [Online]. Available: <https://pubmed.ncbi.nlm.nih.gov/31866339/>.
- [76] V. S. Polikov, P. A. Tresco, and W. M. Reichert, "Response of brain tissue to chronically implanted neural electrodes," *Journal of neuroscience methods*, vol. 148, no. 1, pp. 1–18, 2005.
- [77] K. A. Potter, A. C. Buck, W. K. Self, and J. R. Capadona, "Stab injury and device implantation within the brain results in inversely multiphasic neuroinflammatory and neurodegenerative responses," *Journal of neural engineering*, vol. 9, no. 4, Aug. 2012, ISSN: 1741-2552. DOI: [10.1088/1741-2560/9/4/046020](https://doi.org/10.1088/1741-2560/9/4/046020). [Online]. Available: <https://pubmed.ncbi.nlm.nih.gov/22832283/>.
- [78] A. Roy Lycke *et al.*, "Title Low-threshold, high-resolution, chronically stable intracortical microstimulation by ultraflexible electrodes," DOI: [10.1101/2023.02.20.529295](https://doi.org/10.1101/2023.02.20.529295). [Online]. Available: <https://doi.org/10.1101/2023.02.20.529295>.

- [79] D. J. Edell, V. V. Toi, V. M. McNeil, and L. D. Clark, "Factors influencing the biocompatibility of insertable silicon microshafts in cerebral cortex," *IEEE transactions on bio-medical engineering*, vol. 39, no. 6, pp. 635–643, 1992, ISSN: 0018-9294. DOI: [10.1109/10.141202](https://doi.org/10.1109/10.141202). [Online]. Available: <https://pubmed.ncbi.nlm.nih.gov/1601445/>.
- [80] G. Cellot *et al.*, "PEDOT:PSS Interfaces Support the Development of Neuronal Synaptic Networks with Reduced Neuroglia Response In vitro," *Frontiers in neuroscience*, vol. 9, no. JAN, 2016, ISSN: 1662-4548. DOI: [10.3389/FNINS.2015.00521](https://doi.org/10.3389/FNINS.2015.00521). [Online]. Available: <https://pubmed.ncbi.nlm.nih.gov/26834546/>.
- [81] H. Tashiro, M. B. Popovic, K. Iramina, Y. Terasawa, and J. Ohta, "Direct Neural Interface," *Biomechanics*, pp. 139–174, Jan. 2019. DOI: [10.1016/B978-0-12-812939-5.00006-9](https://doi.org/10.1016/B978-0-12-812939-5.00006-9).
- [82] M. Zhang, Z. Tang, X. Liu, and J. Van der Spiegel, "Electronic neural interfaces," *Nature Electronics* 2020 3:4, vol. 3, no. 4, pp. 191–200, Apr. 2020, ISSN: 2520-1131. DOI: [10.1038/S41928-020-0390-3](https://doi.org/10.1038/S41928-020-0390-3). [Online]. Available: <https://www-nature-com.tudelft.idm.oclc.org/articles/s41928-020-0390-3>.
- [83] C. Kim, J. Jeong, and S. J. Kim, "Recent Progress on Non-Conventional Microfabricated Probes for the Chronic Recording of Cortical Neural Activity," *Sensors 2019, Vol. 19, Page 1069*, vol. 19, no. 5, p. 1069, Mar. 2019, ISSN: 1424-8220. DOI: [10.3390/S19051069](https://doi.org/10.3390/S19051069). [Online]. Available: <https://www.mdpi.com/1424-8220/19/5/1069/htm%20https://www.mdpi.com/1424-8220/19/5/1069>.
- [84] H. Park, P. Takmakov, and H. Lee, "Electrochemical evaluations of fractal microelectrodes for energy efficient neurostimulation," *Scientific Reports*, vol. 8, no. 1, Dec. 2018, ISSN: 20452322. DOI: [10.1038/S41598-018-22545-W](https://doi.org/10.1038/S41598-018-22545-W). [Online]. Available: [https://www.researchgate.net/publication/323702464\\_Electrochemical\\_Evaluations\\_of\\_Fractal\\_Microelectrodes\\_for\\_Energy\\_Efficient\\_Neurostimulation](https://www.researchgate.net/publication/323702464_Electrochemical_Evaluations_of_Fractal_Microelectrodes_for_Energy_Efficient_Neurostimulation).
- [85] A. Kral, F. Aplin, and H. Maier, "Tissue reaction to neuroprostheses," *Prostheses for the Brain*, pp. 135–148, Jan. 2021. DOI: [10.1016/B978-0-12-818892-7.00007-9](https://doi.org/10.1016/B978-0-12-818892-7.00007-9).
- [86] C. R. Butson and C. C. McIntyre, "Role of electrode design on the volume of tissue activated during deep brain stimulation," *Journal of neural engineering*, vol. 3, no. 1, p. 1, Mar. 2006, ISSN: 17412560. DOI: [10.1088/1741-2560/3/1/001](https://doi.org/10.1088/1741-2560/3/1/001). [Online]. Available: [/pmc/articles/PMC2583360/](https://pubmed.ncbi.nlm.nih.gov/pmc/articles/PMC2583360/) [https://www.ncbi.nlm.nih.gov/pmc/articles/PMC2583360/?report=abstract%20https://www.ncbi.nlm.nih.gov/pmc/articles/PMC2583360/](https://pubmed.ncbi.nlm.nih.gov/pmc/articles/PMC2583360/?report=abstract%20https://www.ncbi.nlm.nih.gov/pmc/articles/PMC2583360/).
- [87] X. F. Wei and W. M. Grill, "Current density distributions, field distributions and impedance analysis of segmented deep brain stimulation electrodes," *Journal of Neural Engineering*, vol. 2, no. 4, p. 139, Nov. 2005, ISSN: 1741-2552. DOI: [10.1088/1741-2560/2/4/010](https://doi.org/10.1088/1741-2560/2/4/010). [Online]. Available: <https://iopscience.iop.org/article/10.1088/1741-2560/2/4/010%20https://iopscience.iop.org/article/10.1088/1741-2560/2/4/010/meta>.
- [88] E. Brunton, A. J. Lowery, and R. Rajan, "A comparison of microelectrodes for a visual cortical prosthesis using finite element analysis," *Frontiers in Neuroengineering*, vol. 5, no. SEPTEMBER, Sep. 2012, ISSN: 16626443. DOI: [10.3389/FNENG.2012.00023](https://doi.org/10.3389/FNENG.2012.00023). [Online]. Available: [/pmc/articles/PMC3460534/](https://pubmed.ncbi.nlm.nih.gov/pmc/articles/PMC3460534/) [https://www.ncbi.nlm.nih.gov/pmc/articles/PMC3460534/?report=abstract%20https://www.ncbi.nlm.nih.gov/pmc/articles/PMC3460534/](https://pubmed.ncbi.nlm.nih.gov/pmc/articles/PMC3460534/?report=abstract%20https://www.ncbi.nlm.nih.gov/pmc/articles/PMC3460534/).
- [89] C. C. McIntyre, W. M. Grill, D. L. Sherman, and N. V. Thakor, "Cellular Effects of Deep Brain Stimulation: Model-Based Analysis of Activation and Inhibition," *Journal of Neurophysiology*, vol. 91, no. 4, pp. 1457–1469, Apr. 2004, ISSN: 00223077. DOI: [10.1152/JN.00989.2003](https://doi.org/10.1152/JN.00989.2003). [Online]. Available: <https://journals.physiology.org/doi/10.1152/jn.00989.2003>.
- [90] D. R. McNeal, "Analysis of a Model for Excitation of Myelinated Nerve," *IEEE Transactions on Biomedical Engineering*, vol. BME-23, no. 4, pp. 329–337, 1976, ISSN: 15582531. DOI: [10.1109/TBME.1976.324593](https://doi.org/10.1109/TBME.1976.324593).
- [91] S. Mukesh, D. T. Blake, B. J. McKinnon, and P. T. Bhatti, "Modeling Intracochlear Magnetic Stimulation: A Finite-Element Analysis," *IEEE Transactions on Neural Systems and Rehabilitation Engineering*, vol. 25, no. 8, pp. 1353–1362, Aug. 2017, ISSN: 15344320. DOI: [10.1109/TNSRE.2016.2624275](https://doi.org/10.1109/TNSRE.2016.2624275).

- [92] F. Alonso, *Models and Simulations of the Electric Field in Deep Brain Stimulation : Comparison of Lead Designs, Operating Modes and Tissue Conductivity*. 1945. 2018, p. 174, ISBN: 9789176852613. [Online]. Available: [https://books.google.nl/books/about/Models\\_and\\_Simulations\\_of\\_the\\_Electric\\_F.html?id=4s9tDwAAQBAJ&redir\\_esc=y](https://books.google.nl/books/about/Models_and_Simulations_of_the_Electric_F.html?id=4s9tDwAAQBAJ&redir_esc=y).
- [93] S. Joucla and B. Yvert, "Modeling extracellular electrical neural stimulation: From basic understanding to MEA-based applications," *Journal of Physiology Paris*, vol. 106, no. 3-4, pp. 146–158, May 2012, ISSN: 09284257. DOI: [10.1016/j.jphysparis.2011.10.003](https://doi.org/10.1016/j.jphysparis.2011.10.003).
- [94] A. S. Aberra, A. V. Peterchev, and W. M. Grill, "Biophysically realistic neuron models for simulation of cortical stimulation," *Journal of Neural Engineering*, vol. 15, no. 6, Oct. 2018, ISSN: 17412552. DOI: [10.1088/1741-2552/aadbb1](https://doi.org/10.1088/1741-2552/aadbb1).
- [95] N. A. Pelot, B. J. Thio, and W. M. Grill, "Modeling Current Sources for Neural Stimulation in COMSOL," *Frontiers in Computational Neuroscience*, vol. 12, no. June, pp. 1–14, Jun. 2018, ISSN: 1662-5188. DOI: [10.3389/fncom.2018.00040](https://doi.org/10.3389/fncom.2018.00040). [Online]. Available: <https://www.frontiersin.org/article/10.3389/fncom.2018.00040/full>.
- [96] J. Senk, C. Carde, E. Hagen, T. W. Kuhlen, M. Diesmann, and B. Weyers, "VIOLA—A multi-purpose and web-based visualization tool for neuronal-network simulation output," *Frontiers in Neuroinformatics*, vol. 12, p. 379 000, Nov. 2018, ISSN: 16625196. DOI: [10.3389/FNINF.2018.00075/BIBTEX](https://doi.org/10.3389/FNINF.2018.00075/BIBTEX).
- [97] X. F. Wei and W. M. Grill, "Analysis of high-perimeter planar electrodes for efficient neural stimulation," *Frontiers in Neuroengineering*, vol. 2, no. NOV, p. 635, Nov. 2009, ISSN: 16626443. DOI: [10.3389/NEURO.16.015.2009/BIBTEX](https://doi.org/10.3389/NEURO.16.015.2009/BIBTEX).
- [98] C. inc., "Ac/dc module user's guide," 2020. [Online]. Available: [Available:%20https://doc.comsol.com/5.6/doc/com.comsol.help.acdc/ACDCModuleUsersGuide.pdf](https://doc.comsol.com/5.6/doc/com.comsol.help.acdc/ACDCModuleUsersGuide.pdf).
- [99] S. W. Lee, K. Thyagarajan, and S. I. Fried, "Micro-Coil Design Influences the Spatial Extent of Responses to Intracortical Magnetic Stimulation," *IEEE Transactions on Biomedical Engineering*, vol. 66, no. 6, pp. 1680–1694, Jun. 2019, ISSN: 15582531. DOI: [10.1109/TBME.2018.2877713](https://doi.org/10.1109/TBME.2018.2877713).
- [100] "Itis foundation material database," (accessed: August 23, 2023) [Online]. [Online]. Available: <https://itis.swiss/virtual-population/tissue-properties/database/database-summary/>.
- [101] C. inc., "Comsol's material library," 2023. [Online]. Available: [Available:%20https://doc.comsol.com/5.4/doc/com.comsol.help.matlib/MaterialLibraryUsersGuide.pdf](https://doc.comsol.com/5.4/doc/com.comsol.help.matlib/MaterialLibraryUsersGuide.pdf).
- [102] C. Blog. "Singularities in finite element models: Dealing with red spots." (2015), [Online]. Available: <https://www.comsol.com/blogs/singularities-in-finite-element-models-dealing-with-red-spots/> (visited on 08/24/2023).
- [103] C. Böhler *et al.*, "Multilayer Arrays for Neurotechnology Applications (MANTA): Chronically Stable Thin-Film Intracortical Implants," *Advanced Science*, vol. 10, no. 14, May 2023, ISSN: 21983844. DOI: [10.1002/advs.202207576](https://doi.org/10.1002/advs.202207576).
- [104] E. M. Schmidt, M. J. Bak, F. T. Hambrecht, C. V. Kufta, D. K. O'Rourke, and P. Vallabhanath, "Feasibility of a visual prosthesis for the blind based on intracortical microstimulation of the visual cortex," *Brain : a journal of neurology*, vol. 119 ( Pt 2), no. 2, pp. 507–522, 1996, ISSN: 0006-8950. DOI: [10.1093/BRAIN/119.2.507](https://doi.org/10.1093/BRAIN/119.2.507). [Online]. Available: <https://pubmed.ncbi.nlm.nih.gov/8800945/>.
- [105] F. T. Ulaby and U. Ravaioli, *fundamentals of applied electromagnetics*, 7th ed. Pearson, 2015, ISBN = 978-0-13-335681-6.
- [106] A. Fellner, I. Stiennon, and F. Rattay, "Analysis of upper threshold mechanisms of spherical neurons during extracellular stimulation," *Journal of Neurophysiology*, vol. 121, no. 4, pp. 1315–1328, Apr. 2019, ISSN: 15221598. DOI: [10.1152/JN.00700.2018/ASSET/IMAGES/LARGE/Z9K0031949960014.JPEG](https://doi.org/10.1152/JN.00700.2018/ASSET/IMAGES/LARGE/Z9K0031949960014.JPEG). [Online]. Available: <https://journals.physiology.org/doi/10.1152/jn.00700.2018>.
- [107] S. Joucla and B. Yvert, "The "Mirror" Estimate: An Intuitive Predictor of Membrane Polarization during Extracellular Stimulation," *Biophysical Journal*, vol. 96, no. 9, p. 3495, May 2009, ISSN: 15420086. DOI: [10.1016/J.BPJ.2008.12.3961](https://doi.org/10.1016/J.BPJ.2008.12.3961). [Online]. Available: [/pmc/articles/PMC2711410/%20/pmc/articles/PMC2711410/?report=abstract%20https://www-ncbi-nlm-nih-gov.tudelft.idm.oclc.org/pmc/articles/PMC2711410/](https://pubmed.ncbi.nlm.nih.gov/18800945/).

- [108] C. A. Bossetti, M. J. Birdno, and W. M. Grill, "Analysis of the quasi-static approximation for calculating potentials generated by neural stimulation," *Journal of Neural Engineering*, vol. 5, no. 1, pp. 44–53, Mar. 2008, ISSN: 17412560. DOI: [10.1088/1741-2560/5/1/005](https://doi.org/10.1088/1741-2560/5/1/005).
- [109] D. N. Anderson, B. Osting, J. Vorwerk, A. D. Dorval, and C. R. Butson, "Optimized programming algorithm for cylindrical and directional deep brain stimulation electrodes," *Journal of Neural Engineering*, vol. 15, no. 2, Jan. 2018, ISSN: 17412552. DOI: [10.1088/1741-2552/aaa14b](https://doi.org/10.1088/1741-2552/aaa14b).